International Journal of Coal Science & Technology (2026) 13:44
https://doi.org/10.1007/s40789-025-00859-1

RESEARCH

Control of floor heave with rock bolts-steel piles coupling support technology

Ivan Sakhno[1] · Svitlana Sakhno[1]

Received: 11 April 2024 / Revised: 12 July 2024 / Accepted: 29 December 2025

Abstract

The uncontrolled floor heave in gob-side entry retaining is the serious problem of underground coal mining. This phenomenon has gravely restricted the application of pillarless mining that has been increasingly used in coal mines in recent years. This study proposes rock bolts-steel piles coupling support method to control severe floor heaves in gob-side entry retaining. This study employs finite element method to analyze stress-strain state in surrounding rocks around gob-side entry retaining. It was found that essential floor heave was caused by high horizontal stresses, which were transmitted from the sides of the entry, and vertical delamination of floor strata in the post-peak strains zone under the entry span. These processes complement each other and aggravate the floor heave. This paper proposes four floor reinforcement schemes. As a result of the study, the most effective floor reinforcement scheme was determined, which consists of 3 elements: steel piles installed in the corners of the entry, rock bolts installed between the piles and a steel belt that coupled the bolts in entry floor. The combination of the advantages of floor reinforcement with bolts and steel piles was the basis for the design of rock bolts-steel piles coupling technology. As a result, the post-peak strain and stress areas are the smallest, and floor heave reduces by 80%. Compared with other reinforcement methods, the advantages of rock bolts-steel piles coupling technology were successfully defined in controlling effect.

Highlights

- The main problem of gob-side entry retaining stability is an uncontrolled floor heave, which is a consequence of dilatancy and plastic flow of rocks.
- Essential floor heave is caused by vertical delamination of rocks in the post-peak strains zone under the roadway and extrusion of rocks from under the filling wall.
- Rock bolts-steel piles coupling support technology with parameters based on analysis of the maximum principle strain is crucial for floor heave control.

Keywords Gob-side entry retaining · Floor heave · Rock bolt · Steel pile · Numerical simulation

1 Introduction

The coal mines of US, China, Australia, EU, Turkey and Ukraine use the longwall method as main underground coal mining technique. In this method, the roof strata have caved behind the longwall face, creating a gob. In order to reduce the loss of coal in traditional wide pillars, small coal pillars along the entry were started to use in the 80s. In recent years, the pillarless mining technology has been increasingly used in coal mines (Gao et al. 2019; Zhang et al. (2020); Tian et al. 2020). This technology makes it possible to improve coal recovery ratio, reduce excavation work, reduce panel commissioning time and implement effective Y-shaped ventilation system of the panel.

The pillarless method involves the supporting of entry in different geotechnical circumstances during its life period:

– at the entry development stage in the rock mass in symmetrical stress field;
– at the abutment pressure stage;

✉ Ivan Sakhno
Ivan.Sakhno@mipolytech.education

[1] Technical University "Metinvest Polytechnic" LLC, 80 Pivdenne Shose, Zaporizhzhia 69008, Ukraine

Published online: 28 April 2026

- at the gob-side stage with filling wall along the entry in asymmetrical stress field.

Usually at the last stage a significant asymmetry of the entry deformation is observed. However, the problem of tailgate stability is not completely solved even in the case of filling walls with high bearing capacity. Nowadays a lot of research on gob-side entry roof stability have been carried out and different support schemes have been used. However, the tailgate floor is often not supported and this results to severe floor heave. Dramatic floor heaves have gravely restricted the application of pillarless coal mining.

In controlling of floor heaves in gob-side entry retaining, dinting loaders, such as Hasemag EL160 LS, are widely implemented in actual practice. However, they eliminate the consequences of heaving, and do not influence on the floor heave process; therefore, this method must be repeated periodically, since heaving often occurs again.

Many scholars have studied the floor heave mechanism in gob-side entry retaining (Gong et al. 2017; Li et al. 2023; Yu et al. 2021). Three main floor heave mechanisms in underground coal mine roadways have been indicated: bearing capacity failure, swelling and buckling (Faria Santos and Bieniawski 1989; Mo et al. 2018, 2020). Considering the problem of heaving in gob-side entry retaining, most scholars agree that the key reasons for this phenomenon are high horizontal stresses in immediate floor and the displacement of rocks from under the filling wall. The swelling further complicates the situation in soft rock.

Gong et al. (2017) found that the horizontal stress of the roadway floor is the main factor that directly causing floor heave. Other external factors affect the failure of roadway floor by changing the horizontal stress in the floor. Lin et al. believed (as Gong et al. (2017) reported) that the floor heave in gob-side entry retaining of deep soft rock is a result of the transfer of the "compression effect" in the backfilling body and coal seam, lateral pressure (generated by main roof rotation), compaction of gangue in the gob area, deep high stress, and soft rock swelling pressure. Li et al. 2023 held that the floor heave of entry retaining is caused by concentrated vertical stress in the coal seam and filling wall. The floor is squeezed by the two sides to form an asymmetric sliding force towards the free face of the floor. Moreover, sliding force increases with the increasing of vertical stress. Research results of Yong et al. (2012) presented that bending and folding of floor heave are the main factors in the stage of the first panel mining; floor squeezing plays a great role in the stable stage of gob-side entry retaining; the combination of the two former factors affects mainly the stage of the second mining ahead; abutment pressure is a fundamental contribution to the serious floor heave of gob-side entry retaining, and side corners of solid coal body are key part in the case of floor heave controlling of gob-side entry retaining. Rock bolt orientation in solid coal side was proposed to control the floor heave. Zhang and Shimada (2018) found that the variation of the ratio between the horizontal stresses and the vertical stress in the floor strata is the root cause of the large floor heave. In particular, the influencing of this stress ratio on the floor heave could be divided into three stages: (1) slight influencing stage from 50 m to 16 m before the coal face; (2) intense influencing stage from 16 m before the coal face to 176 m behind the coal face; and (3) slight influencing stage from 176 m to 240 m behind the coal face.

Technologies of floor heave control in gob-side entry:

- closed support system (for example with inverted arch elements);
- stress relief slots (groove or hole);
- floor reinforcement (with grouting or rock bolt).

Closed support system and stress-relief methods are seldom employed in gob-side entry in actual practice. Significant stresses in gob-side entry retaining critically deform the closed support elements, cause heaving and bend the bottom arch element. The reverse arch complicates subsequent repairs of the entry. Stress-relief methods are promising, however, at great depths these methods do not give a good effect. Over time, the floor heave becomes more active, and the fractured rocks in the immediate floor no longer have sufficient bearing capacity. Thus, reinforcement technologies are the most perspective ones. Therefore, the aim of the study is the development of effective floor reinforcement scheme in gob-side entry retaining.

Chang et al. (2014), He et al. (2009), Yang et al. (2019), Wang et al. (2022), Chen et al. (2012), Cao et al. (2016) proposed to control floor heave with hydraulic expansion bolts, rigid rock bolts, flexible anchor supports and coupling support technologies. Rock bolt reinforcement of floor prevents the development of the plastic zone in the floor rock, and controls the delamination of rocks. Shimada et al. (2014), Zhang and Shimada (2018) and Gong et al. (2017) studied the effectiveness of grouting reinforcement on the large floor heave. Usually some additional measures and update of grouting are required. Zheng et al. (2018) designed a composite structure to control the floor heave, which includes concrete inverted arch and rock bolts. Zhai et al. (2017) proposed the combined supporting technology with bolt-grouting and floor pressure-relief that effectively controls the surrounding rock stability of the deep head chamber at Xinzhuang coal mine. Wang et al. (2020) designed a combined support with floor bolt-mesh-shotcrete and 36U-shaped steel round frame to control the floor heave. Xu et al. (2016) proposed to install steel piles in roadway floor corners with a certain interval before the influence of the abutment pressure zone.

Professor Xu is the first who proposed the steel piles in gob-side entry retaining; his contribution is important for the further development of floor heave control methods. However, corner piles create first of all the anti-slide effect. Therefore they do not solve the floor heave problem in the case of gob-side entry retaining at great depth. At the same time traditional rock bolts only reinforce the layered rock in immediate floor, so they also do not solve the floor heave problem in mentioned conditions. Each of these elements counteract to one of at least two main reasons of floor heave problem in gob-side entry retaining. Thus a research gap in this research topic is formed. To overcome this disadvantage in this study rock bolts-steel piles coupling support technology was proposed.

In this paper, floor heave evolution in gob-side entry retaining in the case of pillarless mining was studied. The floor heave fluctuation, stress-strain characteristics of surrounding rocks and support system elements were analyzed with ANSYS code. The numerical modelling process had 6 steps: 1 st step is for roadway in non-mining influenced stage, and 2nd-6th steps are for the gob-side entry retaining. The properties of rock masses with step-by-step simulation were calculated in accordance to the Hoek-Brown failure criterion. This paper proposed four schemes of floor heave control. As a result the most effective floor reinforcement scheme was determined. It had 3 main elements: steel piles, rock bolts and a steel belt. This scheme makes it possible to significantly reduce post-peak strain in floor strata and to control its delamination. Rational parameters of the floor reinforcement scheme were established. As a result, floor heave in gob-side entry retaining decreases by 80%. Flowchart of research is presented in Fig. 1.

2 Engineering background

2.1 Engineering geological conditions

Surgaya coal mine is located in Donbas region of Ukraine. The c_{11} coal seam is typical for South Donbass. The average thickness of the c_{11} coal seam is 1.4 m; the average inclination is 8°.

The 14th eastern panel is arranged in an east direction, with an advancing length of 1600 m. Nowadays, the 14th eastern transport roadway is being developed. The 13th eastern panel was extracted. The current location of mining roadways of 13-14th panels is presented in Fig. 2a. The studied roadway is 14th eastern transport roadway.

Planned position of longwall face and roadways layout during coal mining in 14th eastern panel is presented in Fig. 2b. According to the project, the 14th eastern transport roadway will be mainly used for air intake and main transportation of the longwall face. 13th eastern transport roadway will be reused for air intake and auxiliary transportation of the longwall face. It will be renamed as 14th eastern auxiliary roadway. Y-shaped ventilation will be planned. The retained gob-side 14th eastern transport roadway will be used for air return.

The strata histogram and position of the entry are illustrated in Fig. 2c.

The rock specimens were selected during excavation of the 14th eastern transport roadway. The uniaxial strength tests were completed using a universal testing machine. Then, the deformation modulus (E_{def}) for each specimen was calculated. These results characterize the parameters of intact rock. Methods of laboratory testing and processing of results are given in the previous paper (Sakhno and Sakhno 2023). Test results are shown in Fig. 2c and in Table 1.

Since the surrounding rocks were fissured and discontinuous, the parameters of intact rock were corrected to correspond to rock mass parameters. The Hoek-Brown Failure Criterion (Hoek et al. 2002) was used to calculate the properties of rock masses. Hoek-Brown Parameters: the Geological Strength Index (GSI), values of the constant m_i and the Disturbance factor (D) were determined.

The GSI was calculated from the RMR index (GSI = RMR89–5) (Hoek and Diederichs 2006) based on results of the uniaxial strength tests, the examination of the drill cores, and the observation of rock in the roadway. The six RMR parameters were determined (Bieniawski 1989): strength of intact rock, RQD, spacing of discontinuities, condition of discontinuities, groundwater conditions, effect of discontinuity strike and dip orientation on drivage. During determination of the RMR index the geological documentation was additionally taken into account.

The constant m_i was assumed to be 8 for mudstones, 17 for coal, and 12 for sandstone. The D parameter was assumed to be 0.5 for mudstones and 0 for coal and sandstone, which corresponds to Hoek's classification category (Hoek et al. 2002): "squeezing problems result in significant floor heave, disturbance can be severe unless a temporary invert is placed" and "mechanical excavation in poor quality rock masses (no blasting) resulting in minimal disturbance to the surrounding rock mass" respectively.

Hoek and Diederichs (2006) empirical method was used for calculation of rock mass deformation modulus. The following equation was used:

$$E_{\mathrm{rm}} = E_{\mathrm{i}} \left(0.02 + \frac{1 - D/2}{1 + e^{\left(\frac{60 + 15D - \mathrm{GSI}}{11} \right)}} \right) \tag{1}$$

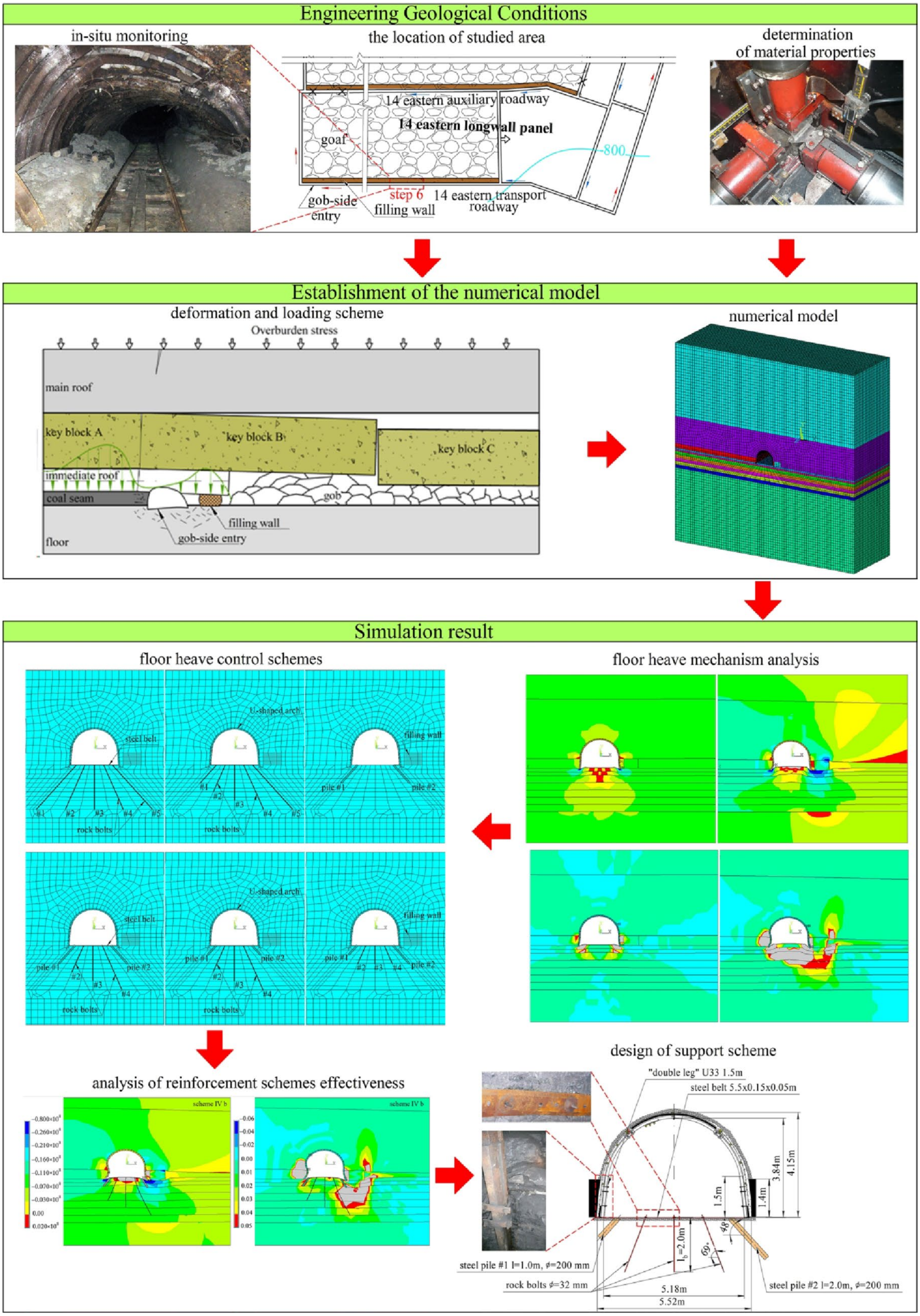

Fig. 1 Flowchart of research

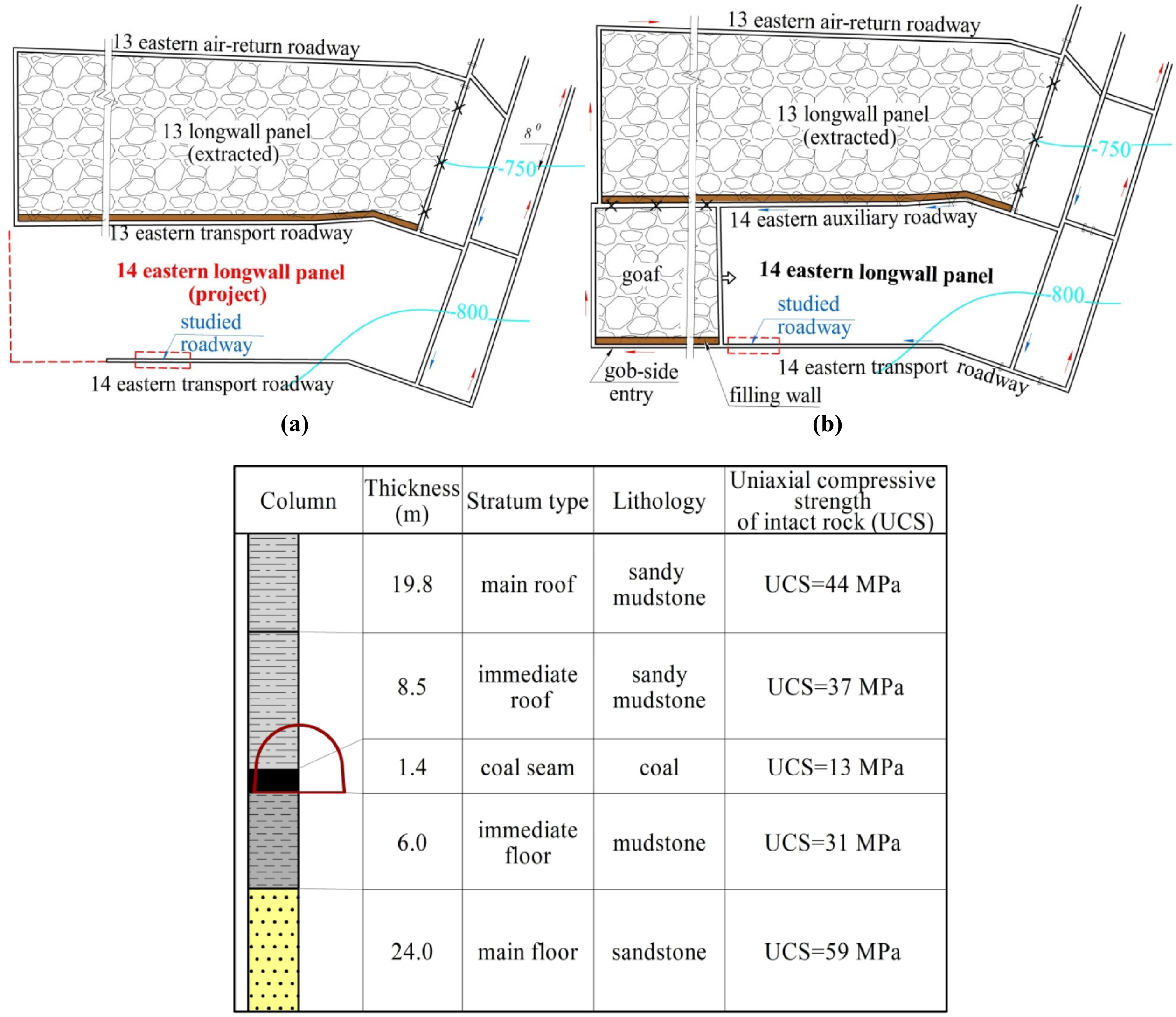

Fig. 2 The studied area and geological conditions: **a** The current locations of mining roadways; **b** The project locations of mining roadways; **c** Strata histogram

Table 1 Intact rock properties and calculated rock mass properties

Rock Strata	Intact rock			GSI/D/m_i	Rock mass		
	Density (kg/m^3)	Deformation modulus (MPa)	Compressive strength (MPa)		Deformation modulus (MPa)	Compressive strength (MPa)	Tensile strength (MPa)
Around gob-side entry							
Sandy mudstone	2400	7100	44.0	52/0.5/8	1191	1.76	0.09
Sandy mudstone	2400	5800	37.0	52/0.5/8	973	1.47	0.08
Coal C_{11}	1300	1970	13.0	35/0/17	224	0.32	0.007
Mudstone	2300	4100	31.0	47/0.5/8	496	0.87	0.04
Sandstone	2400	8900	59.0	55/0.5/12	1804	2.89	0.11
Around head entry							
Sandy mudstone	2400	7100	44.0	57/0.5/8	1625	2.47	0.14
Sandy mudstone	2400	5800	37.0	57/0.5/8	1328	2.07	0.12
Coal C_{11}	1300	1970	13.0	45/0/17	442	0.59	0.012
Mudstone	2300	4100	31.0	57/0.5/8	938	1.74	0.10
Sandstone	2400	8900	59.0	65/0.5/12	3139	5.70	0.25

where E_{rm} and E_i represent the deformation modulus of the rock mass and the intact rock, respectively.

The following equations were used for estimation of the friction angle (φ) and cohesive strength (c) Hoek and Diederichs (2006):

$$\phi = \sin^{-1}\left[\frac{6am_b(s+m_b\sigma_{3n}^{1})^{a-1}}{2(1+a)(2+a)+6am_b(s+m_b\sigma_{3n}^{1})^{a-1}}\right] \quad (2)$$

$$c = \frac{\sigma_{ci}\left[(1+a)s+(1-a)m_b\sigma_{3n}^{1}\right](s+m_b\sigma_{3n}^{1})^{a-1}}{(1+a)(2+a)\sqrt{1+6am_b(s+m_b\sigma_{3n}^{1})^{a-1}/((1+a)(2+a))}} \quad (3)$$

where m_b, s, and a represent peak strength parameters of Hoek-Brown (Hoek et al. 2002);

σ_{ci} – uniaxial compressive strength of the intact rock;

$\sigma_{3n}^{1} = \sigma_{3max}^{1}/\sigma_{ci}$ – the upper limit of confining stress over which the relationship between the Hoek-Brown and the Mohr-Coulomb criteria is considered (Hoek et al. 2002).

The uniaxial compressive strength of the rock mass was calculated as (Hoek et al. 2002):

$$\sigma_{crm} = \sigma_{ci}\, s^{a} \quad (4)$$

The tensile strength of the rock mass was calculated as (Hoek et al. 2002):

$$\sigma_{trm} = -\frac{\sigma_{ci}\, s}{m_b} \quad (5)$$

The properties of the rock mass were calculated for studied strata. They are listed in Table 1.

2.2 Supporting system and deformation characteristics

The section shape of the studied roadway was a semi-circular arch. Its width and height were 5.5 m and 4.2 m respectively. The U-shaped steel arches (SVP-33) with wooden boards as filling material were used in roadway.

Since the 14th eastern transport roadway is still being excavated, the 13th eastern transport roadway was used to analyze the possible deformation characteristics of studied roadway (Fig. 3a). This roadway is located in similar

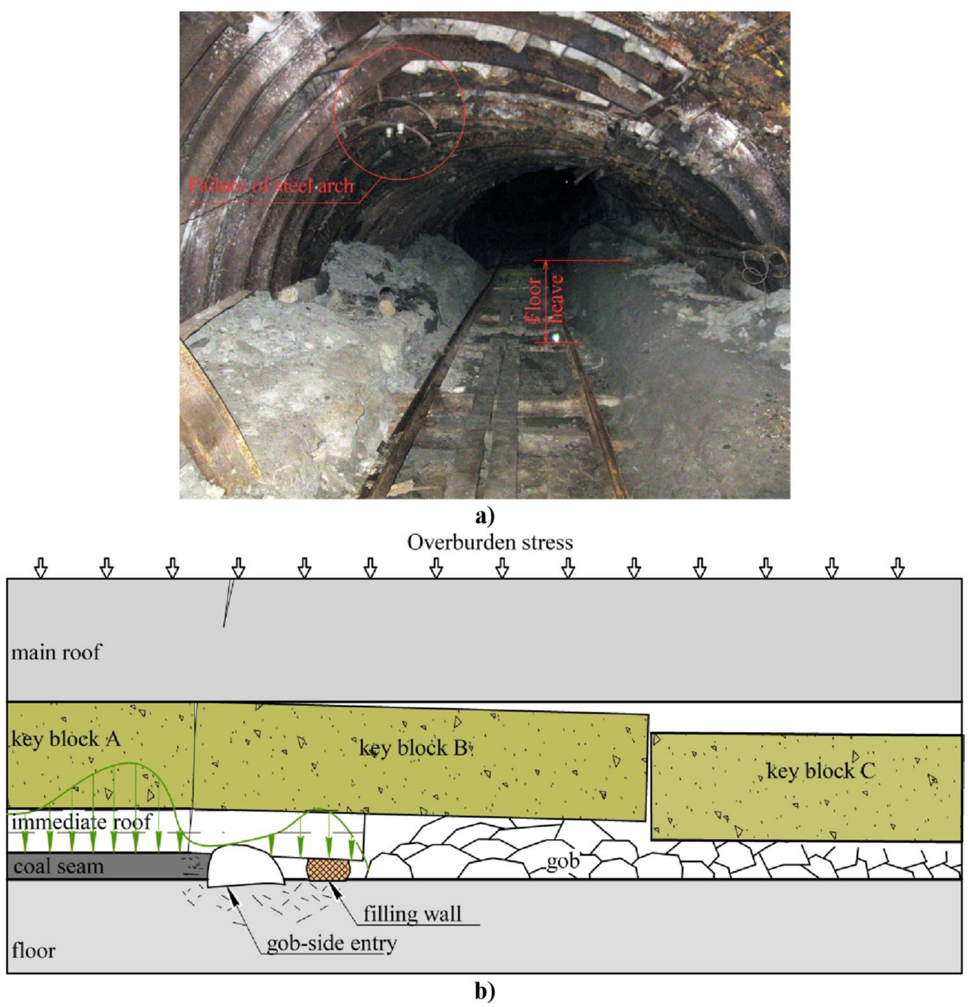

Fig. 3 **a** The characteristics of rupture of gob-side entry retaining; **b** Method of gob-side entry retaining by setting filling material

geological conditions and has an identical support system. The total vertical convergence was about 36% of the initial roadway height; the average floor uplift was 1.18 m; the average roof lowering was 0.29 m. The deformation had a distinct asymmetry in cross section of the roadway. The steel arches were bent and irreversibly deformed. The asymmetric deformation of the steel arches was apparently caused by the impact of the 13th eastern longwall. Most often, the failure of the support was observed in the yielding nodes area of the steel arch from the side of the solid coal seam. A scheme explaining the process of deformation and loading of the gob-side entry retaining is shown in Fig. 3b.

The floor excavation was carried out several times in central part of the retained gob-side roadway to ensure the operation of the auxiliary transport. A lot of effort and material resources were spent on this process. So, the main problem was a floor heave. Therefore in 14th eastern transport roadway it is necessary to optimize the support scheme to control the floor heave of the roadway and ensure the rhythmic and safe operation of the 14th longwall panel.

3 Study of the floor heave of gob-side entry retaining

3.1 Assumptions of the model

The geomechanical situation, in which the studied roadway will be located during exploitation, varies. At the same time, surrounding rock mass fracturing will be increased. For investigation of the floor heave evolution the properties of rock strata were changed in model step-by-step. The numerical modelling process had 6 steps: 1 st step is for roadway in non-mining influenced stage, and 2nd-6th steps are for the gob-side entry retaining (Fig. 4). At the same time the degree of rock mass discontinuity was simulated by changing the Hoek-Brown GSI parameters. For example, the GSI parameter for immediate floor in 1st and 6th steps was GSI = 57 and GSI = 47 respectively. Each next step after the first one GSI was decreased on GSI=−2. Table 2 presents the mechanical parameters of rock mass for each step. Deformation modulus, cohesion value, and angle of internal friction were calculated by Eqs. (1)–(3). The dilatancy angle was taken equal to the angle of internal friction. This corresponded to the unfavorable option. Mechanical parameters of U-shaped steel support are shown in Table 3.

The filling wall is also not a solid body, just like rocks. It has cracks, the number of which also increases with time. Therefore, for the filling wall the same principle of discontinuity accounting (GSI lowering) was applied (as for the rock mass). Such an assumption was made to more adequately simulate the real deformation of the gob-side entry retaining. The properties of filling wall (high-support cemented filling) are shown in Table 4.

3.2 Numerical model

Finite element method is widely used for numerical simulation of mine roadways stability under dynamic and static loads. Software such as ABAQUS (Abdulla et al. 2021) and ANSYS (Sakhno and Sakhno 2023) is used for static analysis, and LS Dyna—for the analysis of dynamic (Deng et al. 2024a) and coupling loads (Deng et al. 2024b).

ANSYS software was used to simulate stress-strain state in surrounding rock. Rock mass, filling wall body, and gangue in goaf are pressure-dependent materials. To simulate their behavior the Drucker-Prager model was used. In previous studies (Sakhno and Sakhno 2023; Liu et al. 2022; Sakhno et al. 2018) was shown that ANSYS Drucker-Prager model is capable to simulate the behavior of the heterogeneous rock mass. The bilinear isotropic hardening model was used to simulate the behavior of U-shaped steel-arch.

The geometric parameters of the model corresponded to the strata histogram (Fig. 2c). The numerical model size was 60 m × 60 m ×20 m (Fig. 4) to minimize boundary effects. The bottom boundary of the model was fixed in vertical, displacement of lateral boundaries were constrained in normal direction. The top boundary was not fixed. The gravity was modeled in vertical direction. Additionally vertical pressure, which was equivalent to the strata weight at the depth of 900 m (22.5 MPa), was applied on the top of the model.

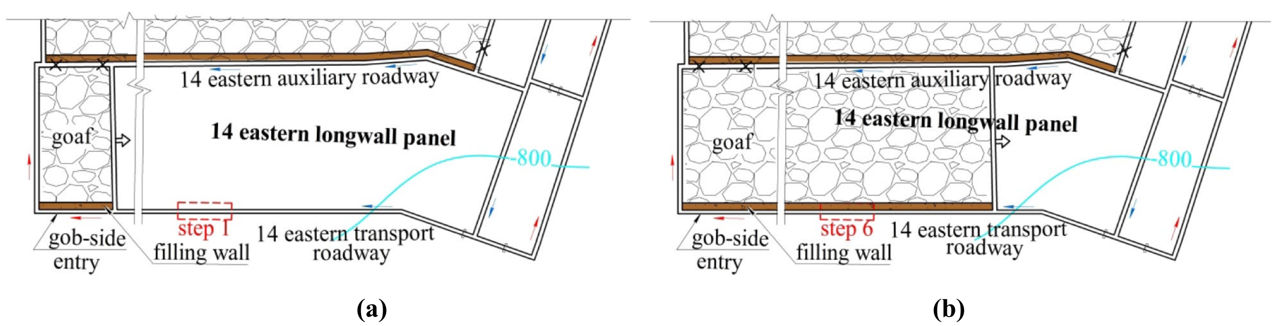

Fig. 4 **a** The location of studied area on 1 st simulation step **b** 6th simulation step

Table 2 Rock mass parameters for numerical simulation

Steps	GSI/*D*	Compressive strength (MPa)	Tensile strength (MPa)	Deformation modulus (GPa)	Poisson's ratio	Cohesion value (MPa)	Angle of internal friction (deg)	Dilatancy angle (deg)
Main roof (sandy mudstone)								
1	57/0.5	2.47	0.14	1.63	0.3	3.59	28	28
2	56/0.5	2.31	0.13	1.53	0.3	3.43	27	27
3	55/0.5	2.16	0.12	1.44	0.3	3.27	26	26
4	54/0.5	2.01	0.11	1.35	0.3	3.11	24	24
5	53/0.5	1.87	0.10	1.27	0.3	2.97	24	24
6	52/0.5	1.75	0.09	1.19	0.3	2.83	24	24
Immediate roof (sandy mudstone)								
1	57/0.5	2.08	0.12	1.33	0.3	3.07	29	29
2	5/0.56	1.95	0.11	1.25	0.3	2.93	29	29
3	55/0.5	1.85	0.10	1.18	0.3	2.80	28	28
4	54/0.5	1.70	0.09	1.10	0.3	2.68	28	28
5	53/0.5	1.58	0.08	1.04	0.3	2.56	27	27
6	52/0.5	1.48	0.08	0.97	0.3	2.45	27	27
Coal seam c_{11}								
1	45/0	0.59	0.012	0.44	0.3	1.51	21	21
2	43/0	0.52	0.010	0.39	0.3	1.42	21	21
3	41/0	0.46	0.009	0.34	0.3	1.33	21	21
4	39/0	0.41	0.008	0.29	0.3	1.26	21	21
5	37/0	0.36	0.007	0.26	0.3	1.19	20	20
6	35/0	0.32	0.006	0.22	0.3	1.13	20	20
Immediate floor (mudstone)								
1	57/0.5	1.74	0.10	0.94	0.3	2.39	24	24
2	55/0.5	1.52	0.08	0.83	0.3	2.20	23	23
3	53/0.5	1.32	0.07	0.73	0.3	2.03	23	23
4	51/0.5	1.15	0.06	0.65	0.3	1.87	23	23
5	49/0.5	1.00	0.05	0.57	0.3	1.73	23	23
6	47/0.5	0.87	0.04	0.50	0.3	1.61	22	22
Main floor (sandstone)								
1	65/0.5	5.70	0.25	3.14	0.3	6.25	35	35
2	63/0.5	4.99	0.21	2.84	0.3	5.73	34	34
3	61/0.5	4.35	0.17	2.56	0.3	5.23	34	34
4	59/0.5	3.80	0.15	2.29	0.3	4.76	34	34
5	57/0.5	3.32	0.12	2.04	0.3	4.32	34	34
6	55/0.5	2.90	0.11	1.80	0.3	3.90	34	34

Table 3 Properties of support elements used in the model

Primary support	Type of elements	Material behavior option	Elastic modulus (GPa)	Poisson's ratio	Yield strength (MPa)	Tangent modulus (GPa)
U-shaped steel support	Beam	Bilinear isotropic hardening	200	0.27	295	52.2
Filling material (wooden boards)	Solid	Isotropic	750	0.3	–	–

The size of the finite element mesh was chosen on the considerations of required accuracy. At the same time analysis results should be in an acceptable time frame. Model areas that were close to entry had the minimal size of the mesh, since high accuracy was important there. Moving away from the entry contour, the mesh size increased. On the contour of the model, the stress field is uniform, so the mesh had the maximum size.

The mesh reducing limit (when further reduce of the mesh size increased the required time to run the analysis without an appreciable increase in accuracy) was established as a result of testing the sensitivity of the model. The maximum size of the finite element was 0.75 m. The minimum size of

Table 4 Filling wall parameters for numerical simulation

Steps	GSI	Compressive strength (MPa)	Tensile strength (MPa)	Deformation modulus (GPa)	Poisson's ratio	Cohesion value, (MPa)	Angle of internal friction (deg)	Dilatancy angle (deg)
Filling wall								
1	–	–	–	–	–	–	–	–
2	79	8.65	0.72	2.29	0.3	4.77	33	–
3	76	7.08	0.50	2.13	0.3	4.48	33	–
4	73	5.79	0.35	1.95	0.3	4.16	32	–
5	70	4.74	0.25	1.75	0.3	3.81	30	–
6	66	3.62	0.16	1.48	0.3	3.33	29	–

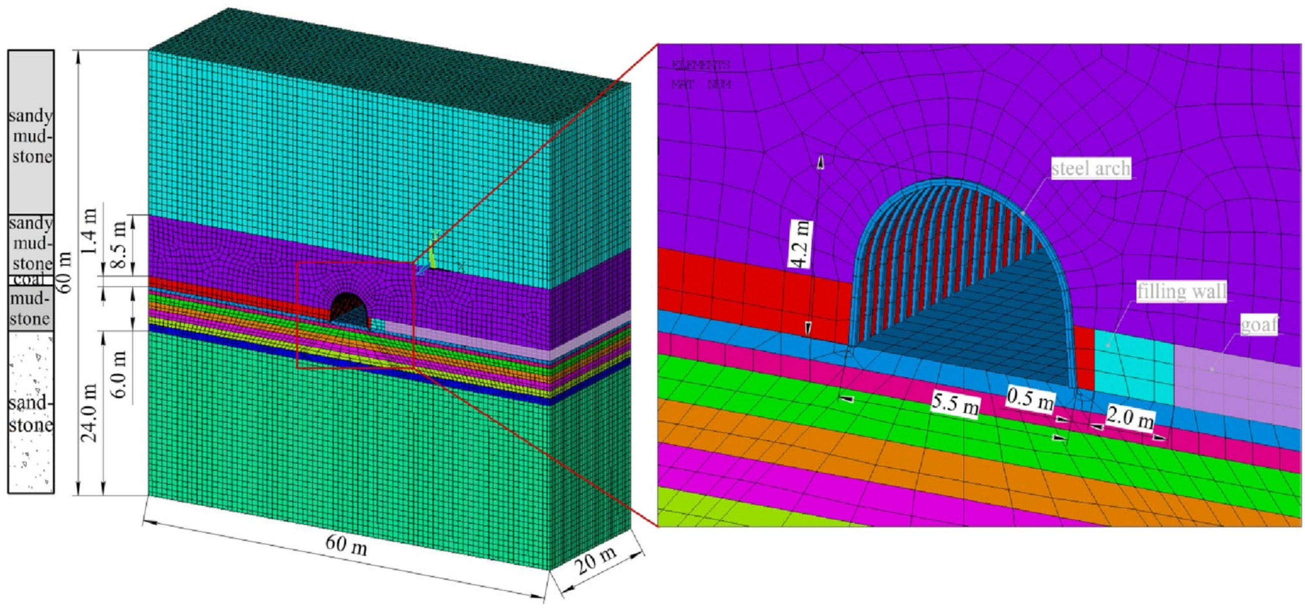

Fig. 5 Numerical model and supporting elements

the finite element was 0.1 m—near the bottom corner of the entry.

A 5.5 × 4.2 m arch-shaped roadway was simulated. The beam element with hat cross section was used to simulate the U-shaped steel support. Between the steel arch and the rock mass the contact surface with friction coefficient 0.45 (dry material) was created. The filling material (wooden boards) was modeled as a plate between rock mass and steel arch. The width of filling wall was 2.0 m, and horizontal distance between wall body and steel arch was 0.5 m (Fig. 5). To simulate the broken gangue in goaf behavior, the following parameters were applied: deformation modulus 30 MPa, and Poisson's ratio 0.45 (Li et al. 2020).

3.3 Simulation results

The simulation of the step-by-step evolution of stress in the surrounding rocks is shown in Figs. 6 and 7. At the first step, the stress distribution is symmetrical to the axis of the roadway (Figs. 6a and 7a), since the roadway is not mining influenced. The analysis of the minimum principal stresses σ_3 (Fig. 6a) shows that an area of increased σ_3 is formed in surrounding rock on the sides of roadway; this is so-called "butterfly zone". The highest σ_3 are formed at the bottom corners of the roadway. The σ_3 in the sidewall and bottom corners of the roadway exceed the compressive strength of the coal and mudstone respectively. There is a high risk of rock failure in these areas. However, floor heave at this step is insignificant – up to 0.2 m.

At the 2nd-6th simulation steps the asymmetry of strains and stresses appears (Figs. 6b, f). This is explained by the load asymmetry for the gob-side entry retaining. The size of the σ_3 increased zone, the value of σ_3 in the sidewalls and floor of roadway increase greatly. Below the filling wall, high compressive stresses occur. These stresses exceed the ultimate strength of the rocks. As the longwall face approaches, the stress concentration in the sides of the roadway decreases, which is explained by the surrounding rock deformations. Steel arch is also deformed asymmetrically. Its maximum curvature is observed in the leg of frame. The

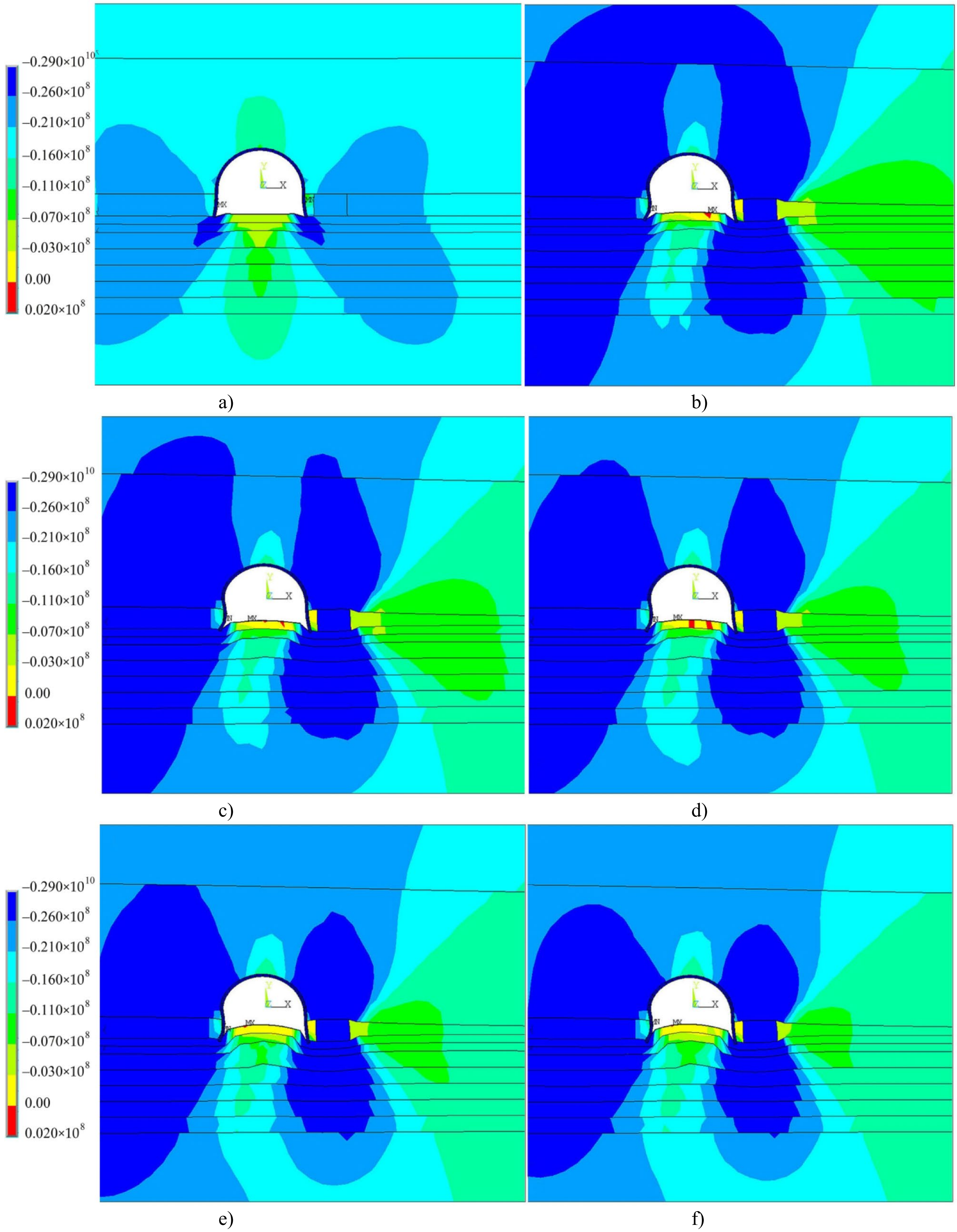

Fig. 6 Minimum principle stress (σ_3) distributions around the roadway with a step-by-step simulation: **a** Step 1; **b** Step 2; **c** Step 3; **d** Step 4; **e** Step 5; **f** Step 6

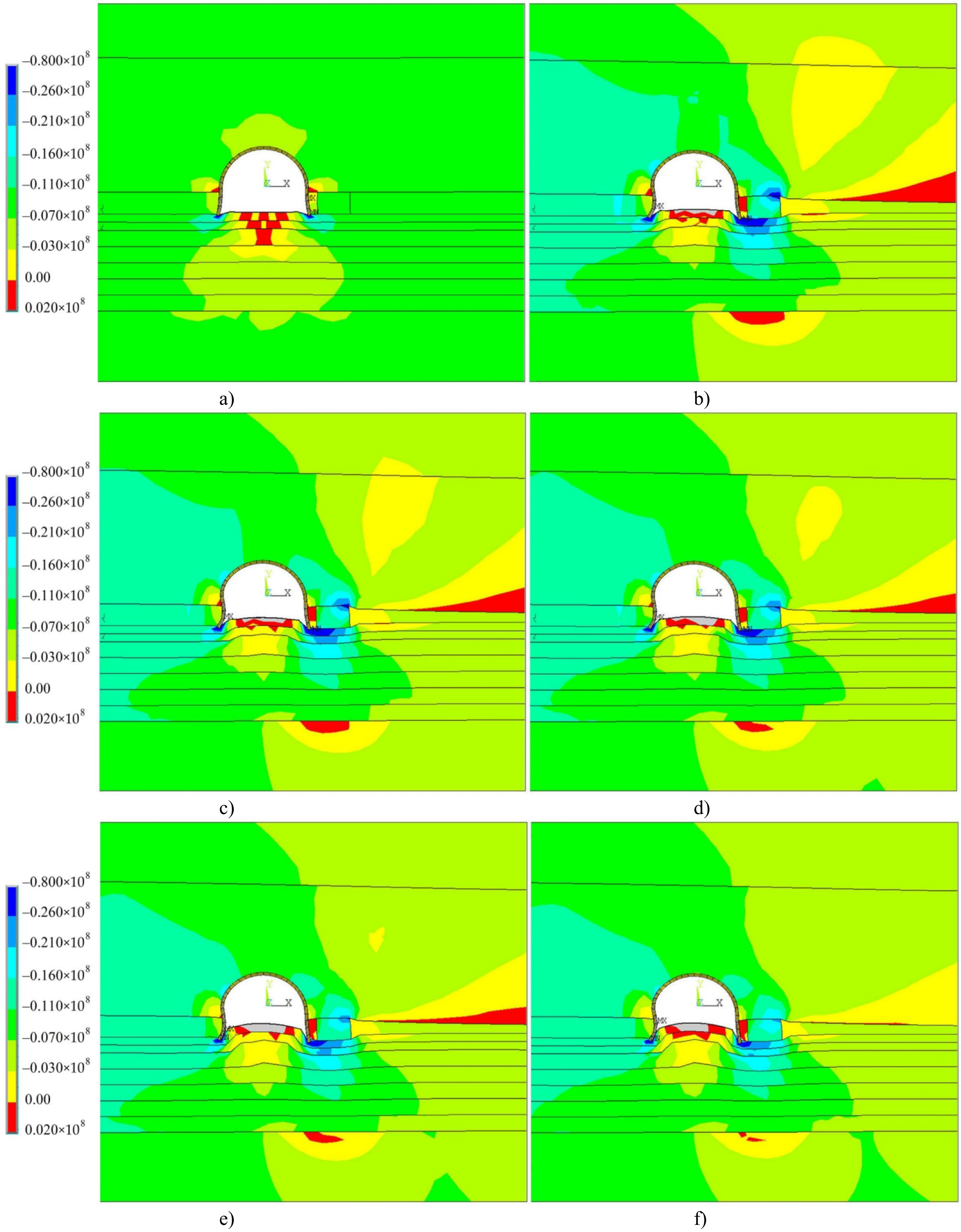

Fig. 7 Maximum principle stress (σ_1) distributions around the roadway with a step-by-step simulation: **a** Step 1; **b** Step 2; **c** Step 3; **d** Step 4; **e** Step 5; **f** Step 6

curved roadway contour becomes similar to the in-situ contour (Fig. 3). Floor heave at 6th step exceeds 1.0 m.

The zone of reduced maximum principal stresses σ_1 is formed in the floor of the roadway at 1 st step (Fig. 7a). At 2nd-6th simulation steps, the stresses σ_1 increase in the mentioned area (Fig. 7b, f). At the 2nd step of the simulation, tensile stresses in immediate floor exceed the tensile strength of mudstone. This potential zone of rock fracture is highlighted in gray color. Insignificant decrease of stress also occurs in the roof. Another zone of critical stresses is formed in the rock strata of the main floor below the filling wall body (Fig. 6b). In this area, the risk of main floor failure is high.

The maximum principle strain distribution is shown in Fig. 8. The results of rock specimen tests show (Sakhno et al. 2018; Sakhno et al. 2023) that failure strain of mudstone and coal are 0.018 – 0.02 and 0.012 – 0.016 respectively. The results of triaxial compression tests (Sakhno et al. 2018; Zhou et al. 2014; Josh et al. 2019) and uniaxial compression (Almisned and Alqahtani 2021; Liu et al. 2021) of sedimentary rocks confirm mentioned strain limits. It was found (Zhou et al. 2014; Josh et al. 2019; Almisned and Alqahtani 2021; Liu et al. 2021) that for mudstone, siltstone, argillite, and sandstone with uniaxial strength of 25 – 40 MPa, the failure criteria for strain is about 0.02 – 0.03. Therefore, in numerical simulation the failure limit was accepted in the range of "−0.02" to "+0.02".

At the first simulation step, strains in the floor and side walls of the roadway exceed the failure limit. This indicates the formation of cracks in the floor. Failure strain areas appear in the bottom corners of the roadway and form closed contour at a depth of about 2.0 m. The surrounding areas with the maximum principle strain, that in 2.5 times higher than the failure limits, in Fig. 8 highlighted in gray color. At this step, the failure strain area is symmetrical with respect to the roadway axis. At the 2nd and subsequent simulation steps, the size of the failure strain area increases significantly. At the same time a clear asymmetry is noticeable. Step by step, the depth of the failure area increases from 2.5 to 4.0 m, and floor heave increases from 0.49 to 1.08 m. Dilatancy and plastic flow evolve in this area, what causes significant floor heave. The potential cracking area covers the rock strata not only in the floor of the roadway, but also below the filling wall body. Thus, the filling wall is vertically pressed into the floor strata. This creates additional horizontal stresses in them. As a result, the heaving becomes more intense. The coal seam in the side of the roadway is also cracked to a depth of more than 1.5 m. The coal failure provokes the bending of the steel arch leg from the side of the solid coal.

The step-by-step evolution of the roadway floor heave is shown in Fig. 9. The non-linear nature of floor heave is clearly seen in the graphs (Fig. 9). According to the floor heave evolution, it can be seen that the value of floor lifting increases non-linearly between 1 st and 2nd steps and between 4th and 5th ones. The floor heave increment between 1 st and 2nd simulation steps is explained by the transition of the experimental roadway part to the gob side. Between 4th and 5th steps the increment is associated with the dilatancy of the near-contour strata (0.5 m thick), which previously displaced without noticeable vertical strains (Fig. 8).

Figure 9 also contains the results of floor heave measuring in 13th eastern transport roadway in non-mining influenced stage and in gob-side retained stage, which corresponds to 1 st and 6th steps of the numerical simulation. Figure 9 shows that the difference between the numerical analysis and field measurements of maximal floor heave are 4.7% and 9.2%, respectively, which allows to conclude that the model is sufficiently reliable.

Figure 10 shows the variation of the strain in the roadway floor at the different simulation steps. As can be seen, horizontal total strains have a minus sign, which means that they are caused by compression. While vertical total strains have a plus sign, which indicates expansion and lamination of rock mass. At the 2nd simulation step, vertical and horizontal strains are higher than the critical ones (± 0.02). Significant vertical expansion of rocks confirms dilatancy in the floor.

The highest vertical strains are observed in the depth range of "−3.0 m" – "−0.5 m". Strains significantly exceed the elasticity limit. This indicates plastic flow in the floor. At the 3rd and 6th simulation steps the vertical strains exceed the elastic limit by 10 and 19 times respectively. Horizontal strains exceed the mentioned limit by 3.5 and 6.5 times on the 3rd and 6th steps, respectively.

In-situ monitoring and the results of numerical analysis allow to get the following conclusions. It is unlikely that floor heave in the 13th eastern transport roadway corresponds to swelling mechanism, since the floor generally was almost dry in the floor areas. The results of the analysis show the key role of horizontal stresses in this process, which allows to conclude that the bearing capacity mechanism can hardly be associated with floor heave. Most likely, floor heave associated with the retreat of the longwall face and roof falls, which induces higher asymmetric stresses compared to the excavation period. The floor failures correspond to buckling. Such findings are consistent with the reported by Mo et al. (Mo et al. 2020) cases of floor heave in Australian mines. Since the main cause of heaving is horizontal stress, it can be concluded that a high degree of deformation is caused by rock mass buckling due to the failure of the floor materials in accordance with Mo et al. (2020) hypothesis.

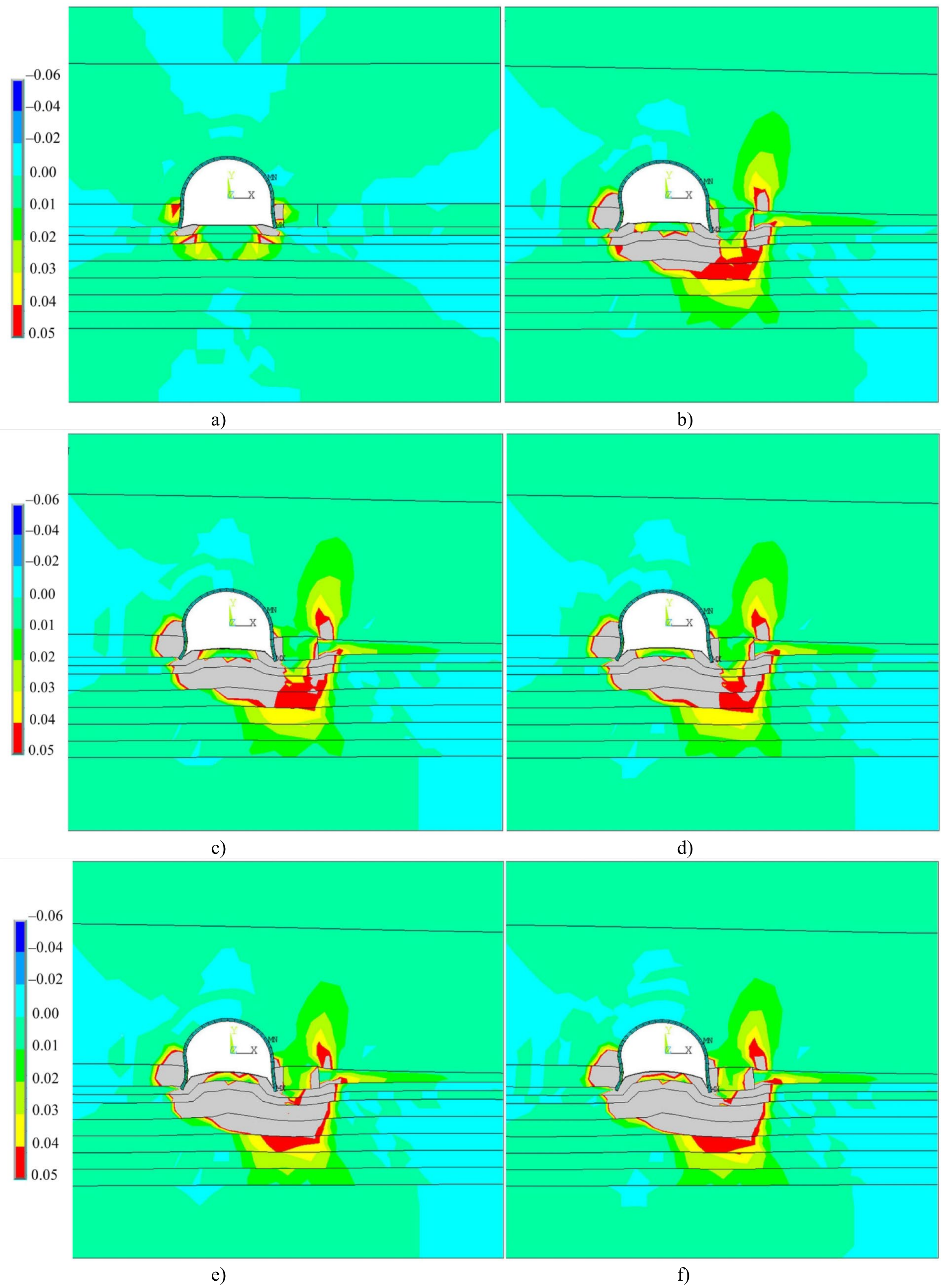

Fig. 8 Total maximum principle strain distributions around the roadway with a step-by-step simulation: **a** Step 1; **b** Step 2; **c** Step 3; **d** Step 4; **e** Step 5; **f** Step 6

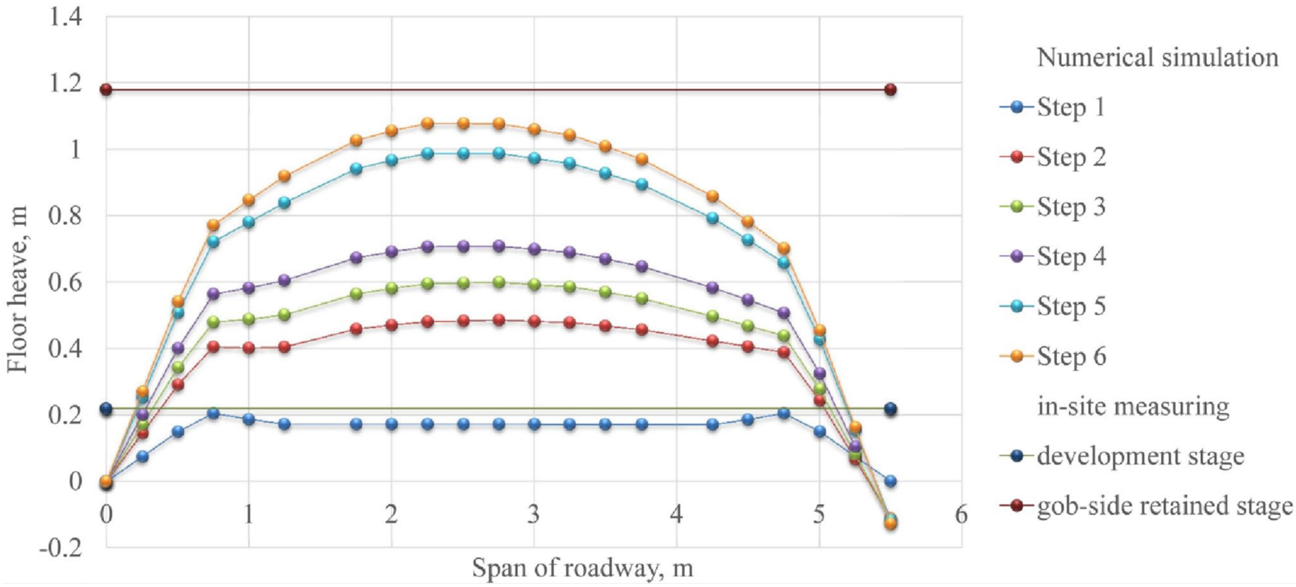

Fig. 9 The roadway floor heave evolution

Fig. 10 The variation in horizontal and vertical total strains with depth at different simulation steps and delamination of floor strata in-situ

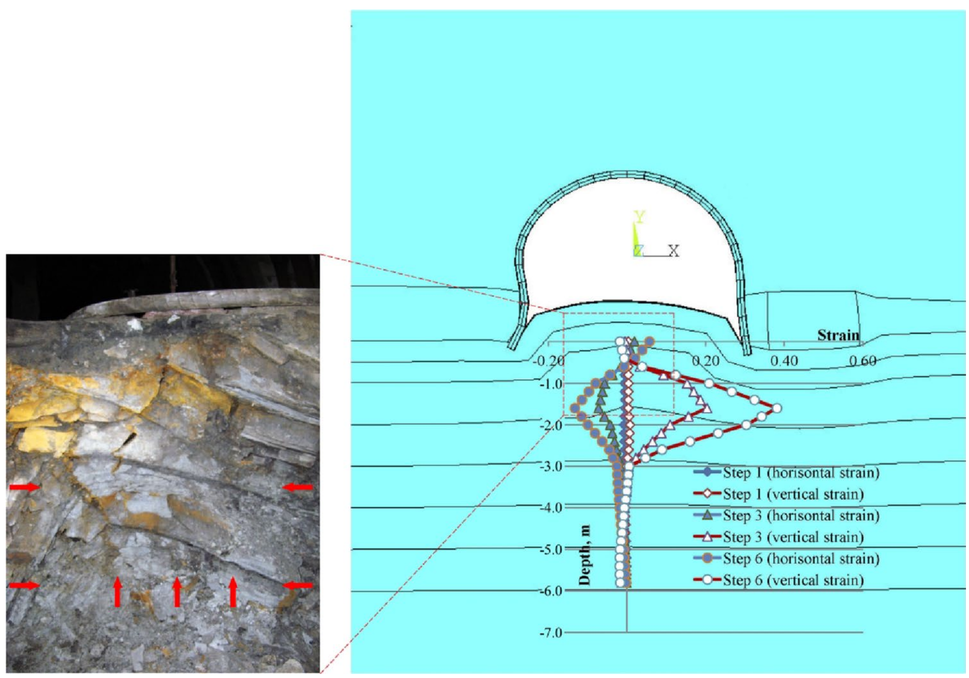

3.4 Simulation discussions

Several conclusions can be drawn according to the above analyses:

(1) The gob-side entry deforms asymmetrically. At the same time, the steel arch bents with irreversible plastic deformation. The axis of the roadway cross section tilted towards the coal body. This is caused by the orientation of the maximum stress vector (Fig. 11). Asymmetry is also observed in the roadway floor. The simulation results correspond with in-situ observations in gob-side entry.

(2) The analysis of the minimum principal stresses σ_3 shows that areas of increased σ_3 are formed on sides of roadway, both on the coal body side and on the filling wall side. Underneath the filling wall, compressive stresses exceed the ultimate strength of the rocks. The filling wall is pressed into the immediate floor. At the same time, the size of the reduced σ_1 stress zone in the floor of the roadway increases significantly. In the non-mining influenced zone (1st simulation step)

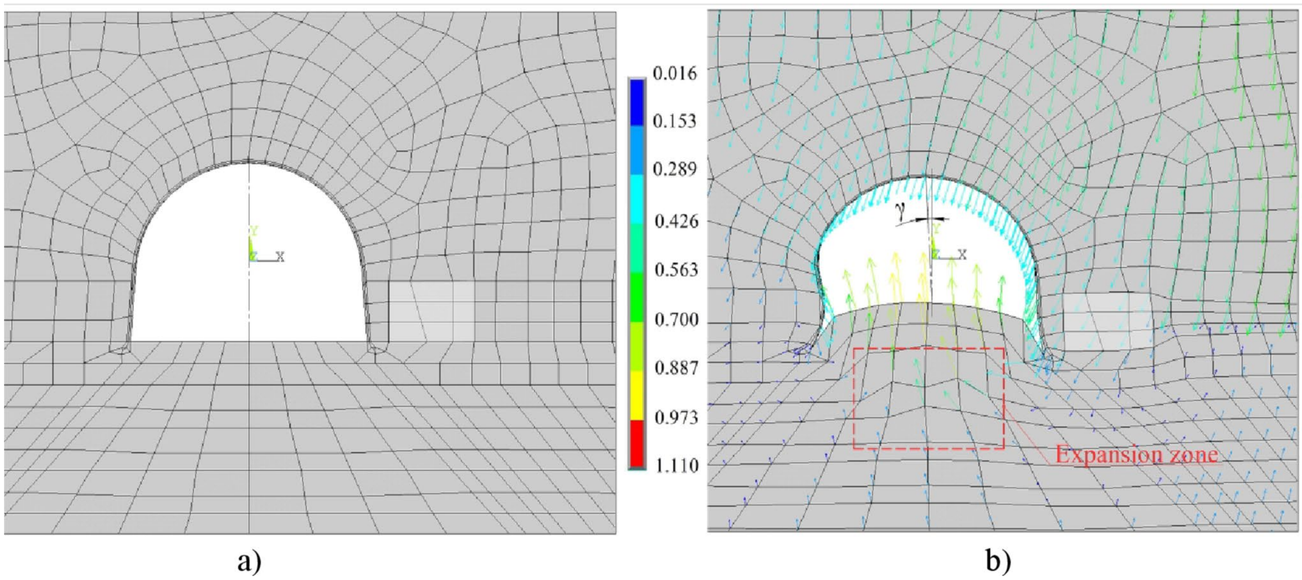

Fig. 11 The simulation of surrounding rock deformation in gob-side entry retaining: **a** The initial state of the model; **b** Displacement vectors on 6th simulation step. Note: γ is inclination of the roadway axis, º.

tensile stresses in the immediate floor exceed the tensile strength of mudstone directly under the roadway span. In retained gob-side roadway (2nd-6th simulation steps) the zone of ultimate stresses is also formed in main floor underneath the filling wall body. The σ_1 in the central part of the roadway floor significantly exceed the tensile strength of floor. This indicates a high risk of rock failure.

(3) The strain analysis shows characteristics of post-peak floor deformations. Failure strain areas appear in the bottom corners of the roadway and form a closed contour at a depth of about 2.0 m. For gob-side entry retaining, the size of the failure strain area increases significantly and covers rocks not only in the floor of the roadway, but also under the filling wall. At the same time a clear asymmetry is noticeable. First of all, a vertical expansion zone with post-peak strains forms in the immediate floor that confirms dilatancy. The plastic flow in the immediate floor also evolves.

(4) The following floor heave mechanism in gob-side entry retaining was proposed. The concentration of vertical stresses leads to the failure of the coal body on one side of the roadway. On the opposite side of the roadway vertically pressured filling wall body leads to the failure of immediate floor underneath it. As a result, horizontal stress increases in the floor strata that causes the extrusion of rocks from under the filling wall into the roadway cavern (Figs. 10 and 11). In addition, vertical delamination of rocks occurs which provokes a critical floor heave. The key to floor heave control is the counteraction to the expansion of rocks in the post-peak strains zone.

(5) Numerical simulation results are valid only for mechanical parameters of rock mass, filling wall, support elements that were applied, and overburden stress at depth 900 m. However, it is clear that the mechanism of floor heave phenomenon will not change significantly in similar geological conditions.

4 Floor heave control technology

4.1 Design of floor heave control schemes

The reinforcement method was proposed for the floor heave control. Fully grouted resin bolts and steel piles were used. Four floor heave control schemes were studied. Firstly, the floor reinforcing design with 5 rock bolts was simulated. The bolts were numbered in the direction from the coal body to the filling wall. The central rock bolt in the row (bolt #3) was located vertically and coincided with the roadway cross section axis. The edge rock bolt (bolt #5) inclination was chosen in such a way as to counteract the vector of maximum strains from the side of the filling wall. At the same time bolt's length was calculated so that its bottom part was located in the pre-peak strains zone (Fig. 12a). Rock bolt #5 was inclined at 48 degrees and bolt #4 was inclined at 69 degrees from the horizontal. The rock bolts orientation was symmetrical about the roadway cross section axis (Fig. 12a). Steel belt was used to couple bolts. The original U-shaped steel arch was not changed. Table 5 shows the mechanical parameters of floor support components in the numerical model.

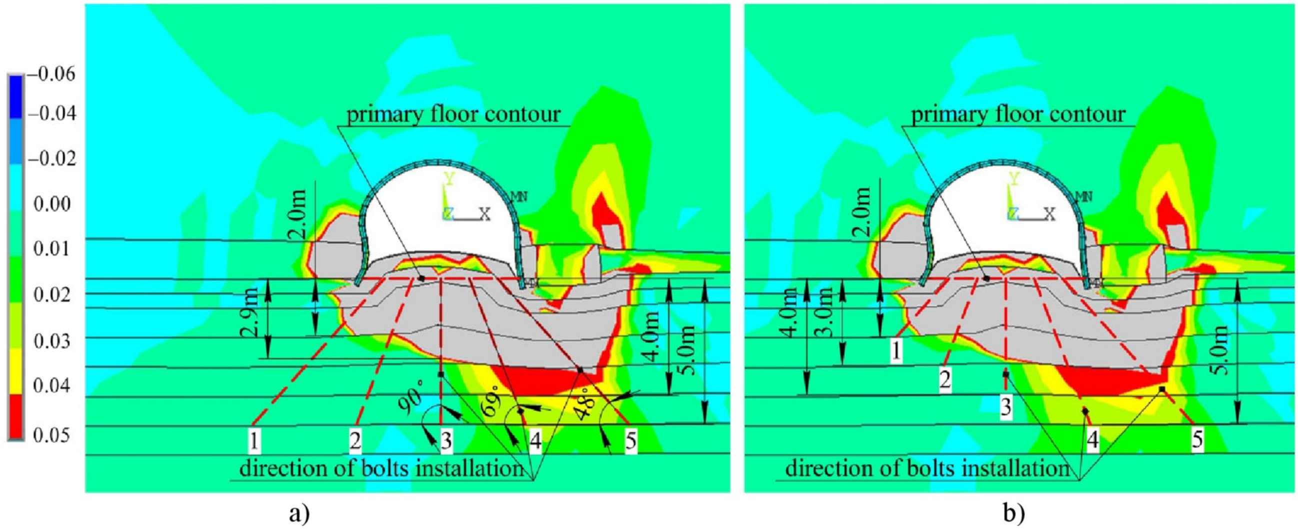

Fig. 12 Total maximum principle strain distributions at 6th simulation step and designed rock bolt floor support schemes: **a** Scheme I; **b** Scheme II

Table 5 Properties of floor support elements used in the model

Floor support element	Elastic modulus (GPa)	Poisson's ratio	Yield strength (MPa)	Tangent modulus (GPa)
Rock bolt (diameter 32 mm)	200	0.27	295	52.2
Steel pile (diameter 200 mm)	200	0.27	295	52.2
Steel belt (width/thickness = 150/5 mm)	200	0.27	–	–

Analysis of the numerical simulation results that were mentioned above (Fig. 8) showed that the area with critical horizontal and vertical strains is limited to a depth of 2.0 m under the steel arch leg from the coal body side, 2.9 m in the central part of the roadway span, and 4.0 m below the steel arch leg from the side of the filling wall (Fig. 12a). Compared to the clear asymmetry of the strain, the stress σ_1 asymmetry was not significant (Fig. 7f).

Two rock bolt support schemes were modeled. Scheme I was a symmetrical one with constant depth of reinforcement. The maximum vertical depth of the reinforcement area was 5.0 m (Fig. 12a). Scheme II was provided for the use of bolts with different lengths, in accordance with the shape of the post-peak strain area. Taking into account necessary safety factor, the vertical depth of reinforcement was: bolt #1–2.0 m, bolt #2–3.0 m, bolt #3–4.0 m, bolt #4–5.0 m, bolt #5–5.0 m (Fig. 12b).

According to scheme III two steel piles were installed in the floor corners. Study of Xu et al. (2016) showed the high efficiency of the floor heave control method with steel pile in gob-side entry retaining. This paper served as inspiration for the current study. The diameter of the piles was 200 mm and the length was 2.0 m in this study. The piles were numbered in the direction from the coal body to the filling wall (as well as bolts). The axes of the piles coincided with the axes of the bolts, so pile #1 coincided with bolt #1, and pile #2 coincided with bolt #5 from the previous schemes (Fig. 12). The central part of the roadway span remained unreinforced. The mechanical parameters of steel pile are shown in Table 5.

The integration of rock bolts and piles technologies was the basis for Scheme IV. Combining the effects of counteraction to horizontal stresses, which were transmitted from the sides of the roadway, and delamination of floor strata was the main idea of rock bolts-steel pile coupling support technology. This idea is realized in floor heave support scheme IV. In this case, scheme IV was modeled in three variants:

IVa—2.0 m long steel piles coupled with three rock bolts (#2, #3, #4) of different lengths (as in scheme II);

IVb—1.0 m long steel piles coupled with three rock bolts (#2, #3, #4) of different lengths (as in scheme II);

IVc—1.0 m long steel pile #1 and 2.0 m long steel pile #2 coupled with three short bolts (bolting depth of 2.0 m).

Figure 13 shows the support schemes that were studied

4.2 Effectiveness of reinforcement

Firstly, rock bolts reinforcement according to scheme I was modeled. The distribution of minimum principal stresses (σ_3) around the roadway at the 6th simulation step before and after bolt reinforcement is shown in Figs. 14a, b, respectively. It can be seen that bolting does not solve the problem of stress asymmetry. The size of increased minimum principle stresses (σ_3) zones in the sides and floor of the roadway is varied insignificantly. However, the stress in the steel arch increases after floor reinforcement. Thus, the maximum stress (σ_3) increases from 2.78 GPa to 4.25 GPa. The steel arch legs are critically bent and plastically deformed. Steel arch deformations after floor reinforcement

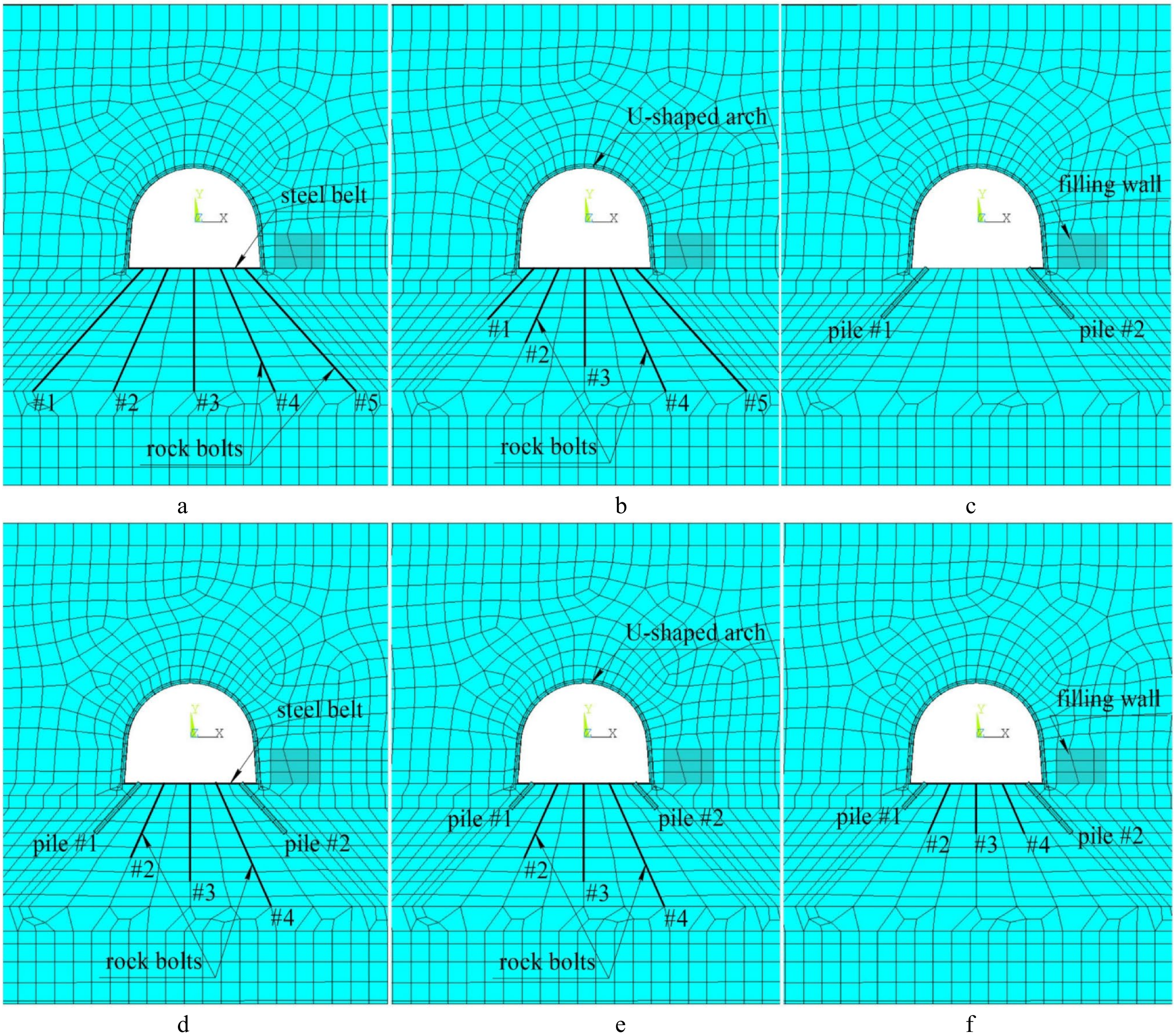

Fig. 13 Finite element models for different floor heave control schemes: **a** Scheme I; **b** sScheme II; **c** Scheme III; **d** Scheme IVa; **e** Scheme IVb; **f** Scheme IVc

are more significant than before reinforcement. While before floor bolting dramatic curvatures of the steel arch legs are observed mainly from the side of the coal body, after reinforcement the steel arch leg from the side of the filling wall is also bent significantly. Since the floor heave after reinforcement decreases substantially, and the stresses (σ_3) in the surrounding rocks do not varied significantly, it can be concluded that during the floor bolting, the stresses (σ_3) do not have a considerable impact on the heaving.

A far greater influence of floor bolting is observed in the distribution of maximum principle stress (σ_1), as can be seen in Figs. 14c, d. After the reinforcement, the size of the relieved stress (σ_1) area in the floor strata is significantly reduced. The critical stress σ_1 area decreases and transits towards the filling wall. This indicates a high responsiveness of tensile stresses in the floor strata (which are largely the cause of heaving) to reinforcement. The positive reinforcement effect can be traced most clearly by analyzing the variation of the maximum plastic principle strain around the roadway. It can be seen that floor bolting significantly changes the geometry of the plastic deformation zone, substantially reducing its size. This is reflected in the reduction of floor heave.

The post-peak plastic strains below the central part of the roadway span practically disappear after reinforcing. However, they still remain in the floor strata underneath the filling wall and on the sides of it. Prevention of dilatancy and plastic flow in this zone by reinforcement is not achieved.

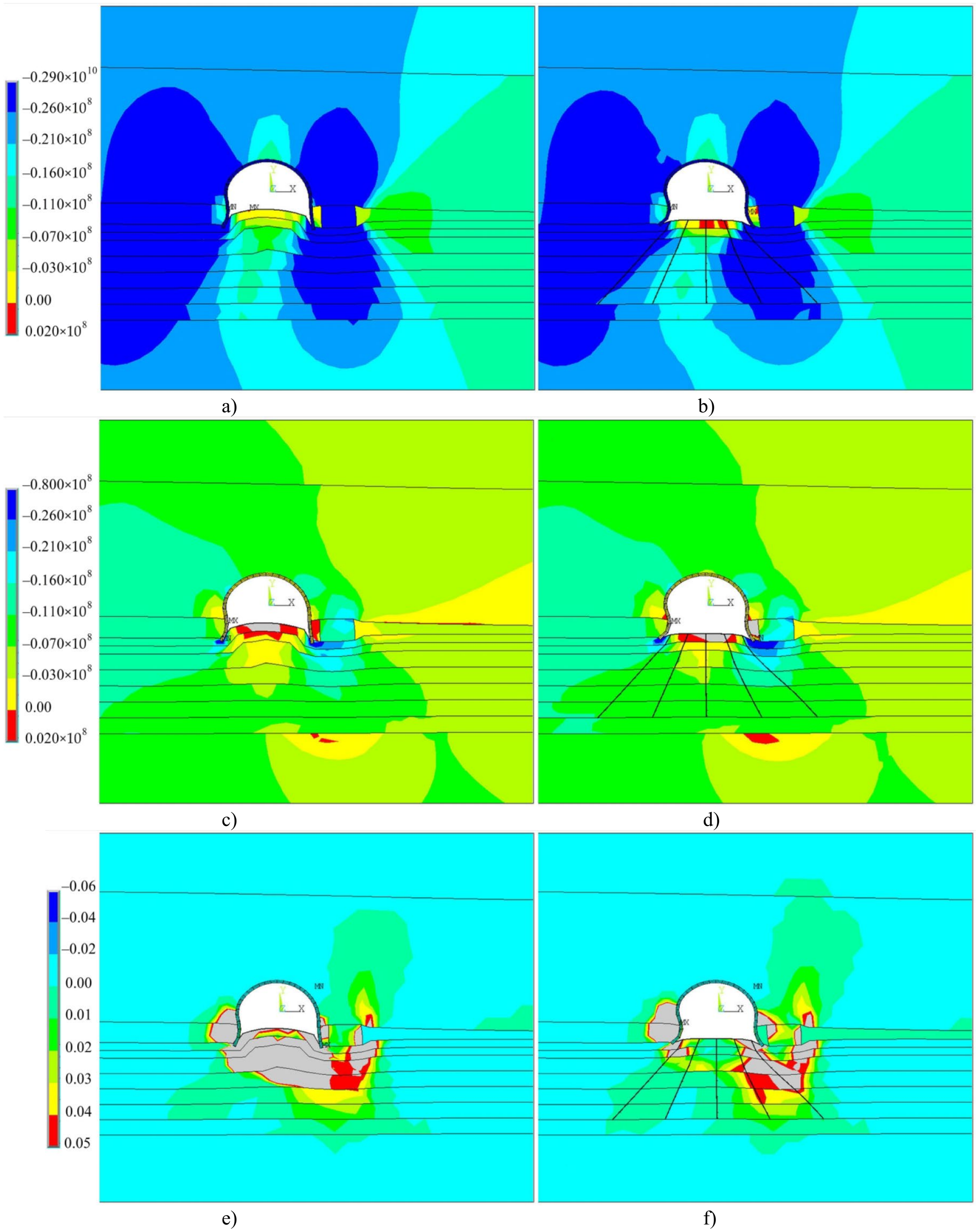

Fig. 14 Minimum principle stress (**a**, **b**), maximum principle stress (**c**, **d**) and maximum principle plastic strain distributions (**e**, **f**) around the roadway at 6th simulation step before and after bolt reinforcement (scheme I)

The graphs of roadway floor heave evolution with a step-by-step simulation are shown in Fig. 15. The figure also shows total maximum principle strain distribution around the roadway. Comparison of floor heave value before (Fig. 9) and after (Fig. 15) bolting shows that reinforcement significantly reduces floor heave. However, the reinforcement efficiency is different at each simulation step. So, at the 1 st simulation step, floor heave on average decreases by 16%, at the 2nd - by 63%, at the 3rd - by 67.8%, at the 4th - by 68.8%, at the 5th, 6th - by 73%.

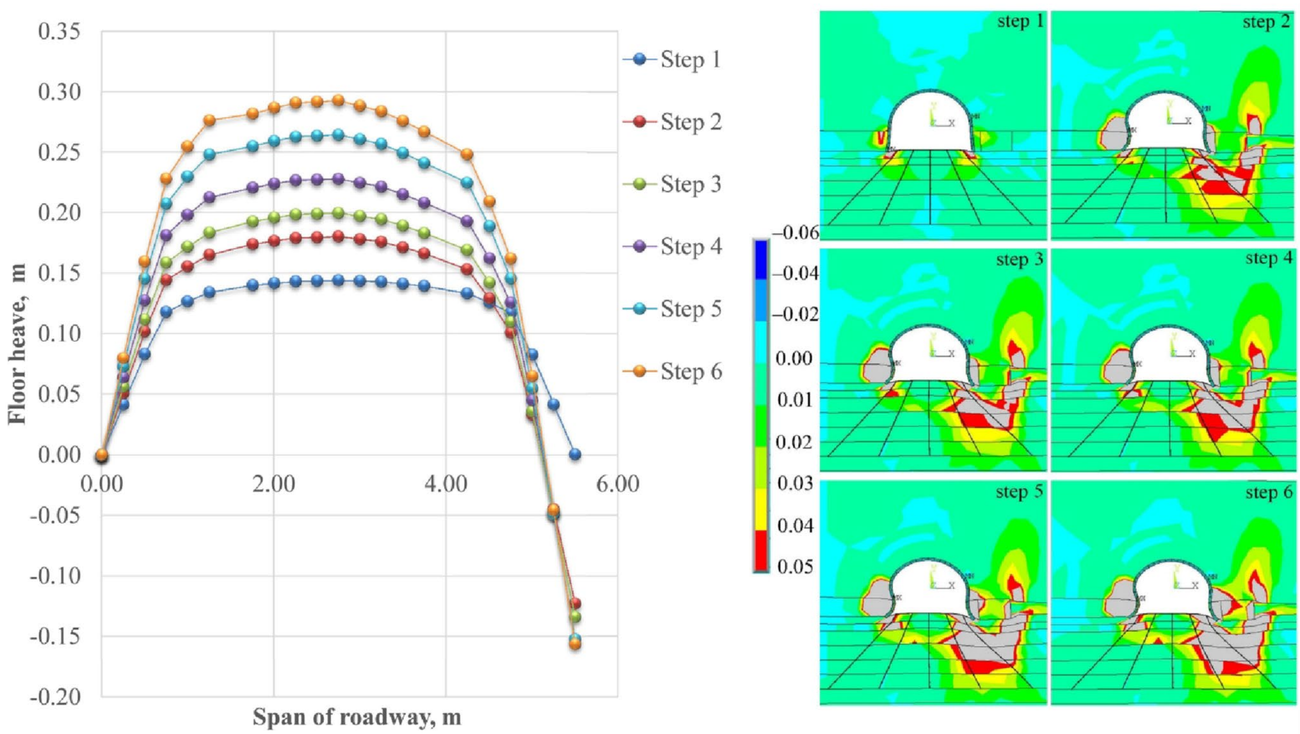

Fig. 15 **a** The roadway floor heave evolution and **b** Total maximum principle strain distributions around the roadway with a step-by-step simulation after bolt reinforcement (scheme I)

The floor bolting have caused substantial reduction of the post-peak strains area. After that this area does not cover the rocks under the roadway span. Significant excesses of the strain limit are observed under the filling wall body nearby bolt #4 and bolt #5 (Fig. 15). In this area plastic flow and dilatancy of rock strata occur. Variations of the horizontal and vertical strains below the central part of the roadway span before and after floor bolting are shown in Fig. 16a. The vertical strains, which directly determine the heaving, decrease from 0.38 to 0.02, as can be seen from Fig. 16a. After reinforcement the area of post-peak vertical strains under the roadway span does not appear. Local areas of insignificant post-peak vertical strains occur between the bolts (Fig. 16b). Horizontal strains also reduce from 0.13 to 0.03. This means that a slight excess of post-peak stresses still appears even near the rock bolts. However, it is clear that reinforcement reduces the vertical and horizontal strains, controls the delamination of the rock strata.

After that, asymmetrical bolt reinforcement scheme (scheme II) with different bolts lengths was modeled. The result of simulation is shown in Fig. 17. Comparison of stress distributions around the roadway after reinforcing in accordance with scheme I (Fig. 17a) and with scheme II (Fig. 17b) shows that there are no significant differences. A similar conclusion can be drawn by analyzing the distribution of principle strains (Figs. 17c, d). Thus, the asymmetric bolting scheme does not worsen the stress-strain state around the gob-side entry retaining. At same time in scheme II bolt #1, bolt #2, bolt #3 are shorter than in scheme I. Less material consumption makes scheme II more preferable. Floor heave after bolt reinforcement in scheme I and scheme II differs insignificantly (Fig. 18). There is every reason to assume that scheme II is more rational. However, it should be noted that the parameters of the scheme, such as the length and number of bolts, must be set in each case separately, depending on the properties of the rocks, parameters of U-shaped steel support, filling wall material and mining depth.

An analysis of the simulation results shows that under the filling wall near bolt #5, an area of post-peak strains still appears (as in scheme I). In addition, bolt #5 and bolt #1 critically bend in under horizontal stresses. To counteract these stresses, according to floor heave control scheme III, two steel piles were installed in the roadway corners (Fig. 13c).

Figure 18 shows the distribution of maximum principle stress (Fig. 18a) and maximum principle strain (Fig. 18b) around the roadway at the 6th simulation step after steel pile installation. Maximum principle stress in the floor strata after steel piles installation is slightly less than after bolt reinforcement. However, in this case, floor heave has a clear asymmetrical character along the roadway span and larger

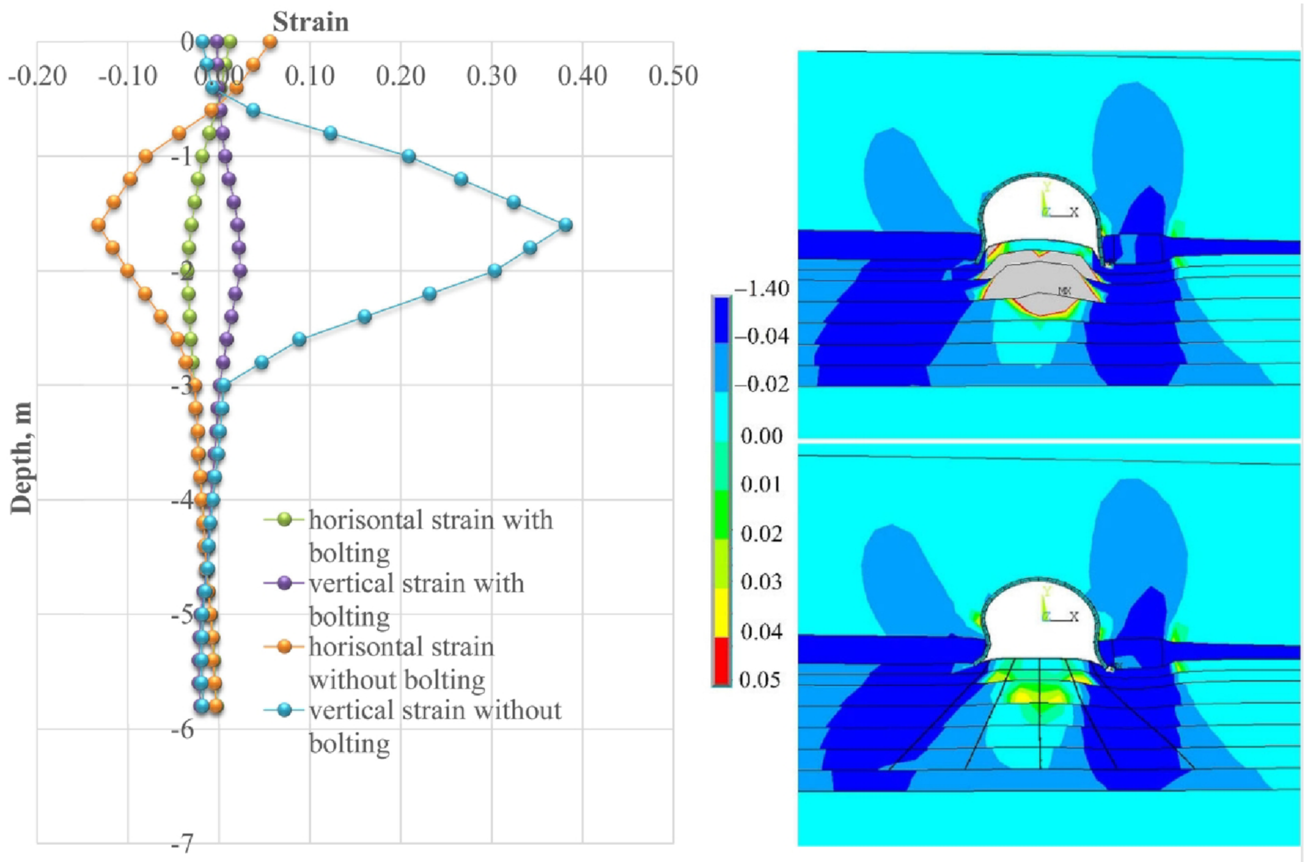

a) b)

Fig. 16 **a** The variation in horizontal and vertical total strains with depth in central part of the roadway span and **b** Vertical strain distributions around the roadway at 6th simulation steps before and after bolt reinforcement (scheme I)

absolute value then after bolt reinforcement (Fig. 18a). The result of this is a decrease of maximum stresses in the immediate floor. On the other hand, steel piles installation increases the compressive stresses in immediate floor under the filling wall and underneath the steel arch leg on the side of the coal body, which indicates their sufficient counteraction to displacement of rock. The pile on the coal body side does not bend like a bolt, but on the filling wall side it is still slightly bent.

Analysis of maximum principle strain (Fig. 18b) distributions shows that the post-peak strain area after piles installation is larger than in the case of bolt reinforcement. Between the piles, the post-peak strains significantly exceed the critical ones. In the result, vertical delamination of rocks and their displacement into the roadway cavern occurs. Area of significant post-peak strains between the piles located at a depth of 1.0–2.2 m (Fig. 18c). Horizontal strains reduce to 0.08, which is 38% less than before the piles installation, but three times higher than after the bolts reinforcement. It is clear that steel piles restrain horizontal stresses in the floor, which were transmitted from the sides of the roadway, much better than bolts. But they do not counteract to vertical delamination of immediate floor in the central part of the roadway span. A comparison of vertical strain distributions around the roadway after bolting and piles installation (Fig. 18d) shows that after piles installation in the central part of the roadway span (at a depth of 1.0–2.2 m) vertical strains form the rock expansion core which was not there after bolt installation.

The combination of the advantages of floor reinforcement with bolts and steel piles was the basis for the design of rock bolts-steel pile coupling technology. This technology was modeled in three variants of scheme IV (Figs. 13d, e, f).

The distribution of maximum principle stress and maximum principle strain around the roadway at the 6th simulation step after reinforcement with scheme IV is shown in Fig. 19.

Floor heave has symmetrical form along the roadway span after reinforcement with scheme IV. Maximum principle stress in the floor strata in all three variants of reinforcement scheme IV varied slightly (Figs. 19a, c, e). In this case, the stress distribution is more favorable in comparison with previous floor reinforcement schemes. Analysis

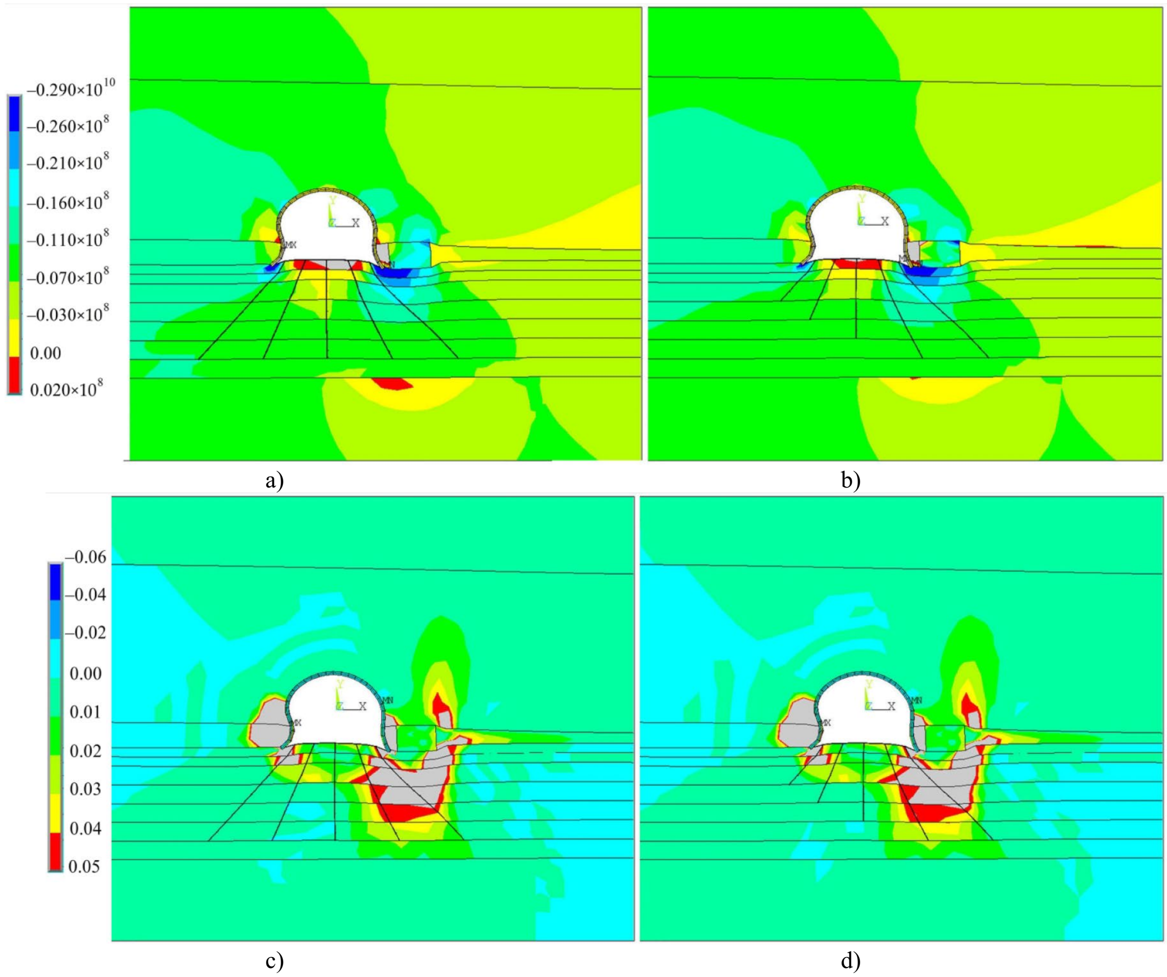

Fig. 17 **a**, **b** Maximum principle stress and **c**, **d** Maximum principle strain distributions around the roadway at 6th simulation step after bolt reinforcement with scheme I and scheme II

of maximum principle strain distributions (Figs. 19b, d, f) leads to similar conclusion. The post-peak strain area under the steel arch leg on the coal body side does not occur, as in the case of steel piles installation. The size of the post-peak strain area on the side of the filling wall and in the center of the roadway span is significantly reduced compared to all previous schemes. The worst variant of scheme IV is scheme IVb, in which both piles have a length of 1.0 m. In this case, the dimension of the post-peak strain area near the pile #2 is the largest of all scheme IV variants (Fig. 19d). At the same time, a comparison of schemes IVa and IVc shows that there is no significant difference in the stress and strain distributions between them. However, in scheme IVc bolts #2, #3, #4 are shorter than in other schemes and steel pile #1 is 1.0 m long. This means that consumption of support elements is less than in other variants of scheme IV that makes this variant more favorable.

Graphs of floor heave in gob-side entry retaining for different reinforcement schemes are shown in Fig. 20. Floor heave is minimal after reinforcement with scheme IV. However, there is no significant difference between IVa, IVb, IVc variants. In summary, scheme IV is the most effective because it provides a reduction in floor by 80%. The simulation result shows that scheme IVc is the most effective for floor heave counteraction in gob-side entry retaining.

4.3 Rock bolts-steel piles coupling support scheme

The main problem of gob-side entry retaining stability in Surgaya coal mine is a dramatic floor heave. The current support system of the entry should be improved. The effective mining of 14th longwall panel requires modification of floor heave support technology. Based on results of numerical simulation, the most effective scheme (scheme IVc, Fig. 12f) of floor reinforcement was proposed additionally to original support system. Diameter of rock bolts was 32 mm, of steel piles – 200 mm. Steel belt 150 × 5 mm was used during rock bolts reinforcement. Numerical simulation shows that steel arch legs bent more after reinforcement than before it. Therefore double steel arch legs with length

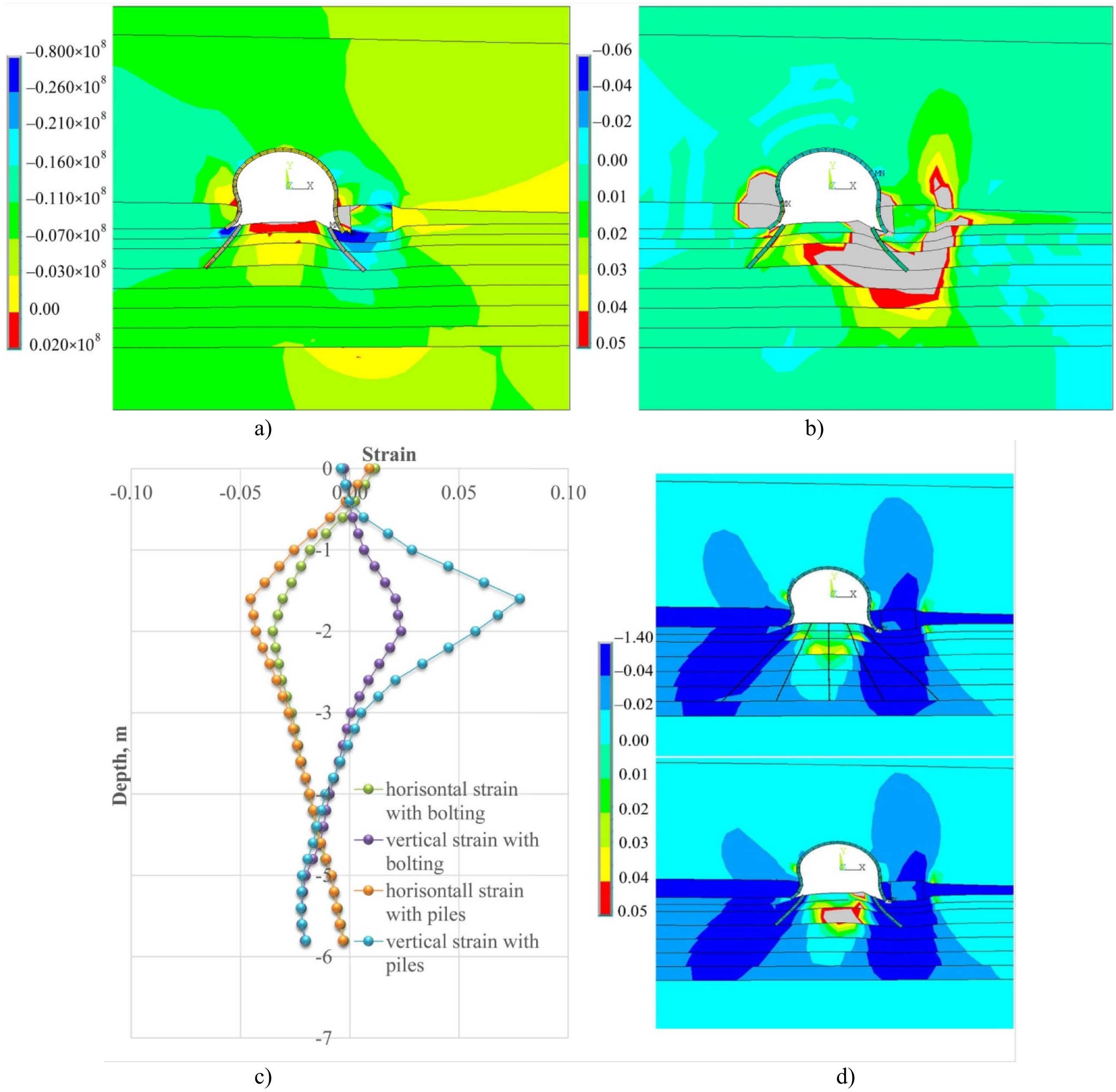

Fig. 18 **a** Maximum principle stress and **b** Maximum principle strain distributions around the roadway at 6th simulation step after reinforcement with scheme III; **c** The variation in horizontal and vertical total strains with depth in central part of the roadway span; **d** Vertical strain distributions around the roadway after bolting and pile installation

1.5 m were proposed. Figure 21 shows the proposed design of support scheme.

5 Conclusions

This study was focused on the mechanism of floor heave evolution and its control by the different reinforcement technologies. The gob-side entry retaining of deep coal mine was considered as the research subject. A finite element method was used to study the stress-strain state of surrounding rock strata. Based on the results of this investigation, the following conclusions can be drawn:

(1) The floor heave in gob-side entry retaining is caused by two main reasons, which complement each other:

   – high horizontal stresses, which were transmitted from the sides of the entry to floor strata. At the same

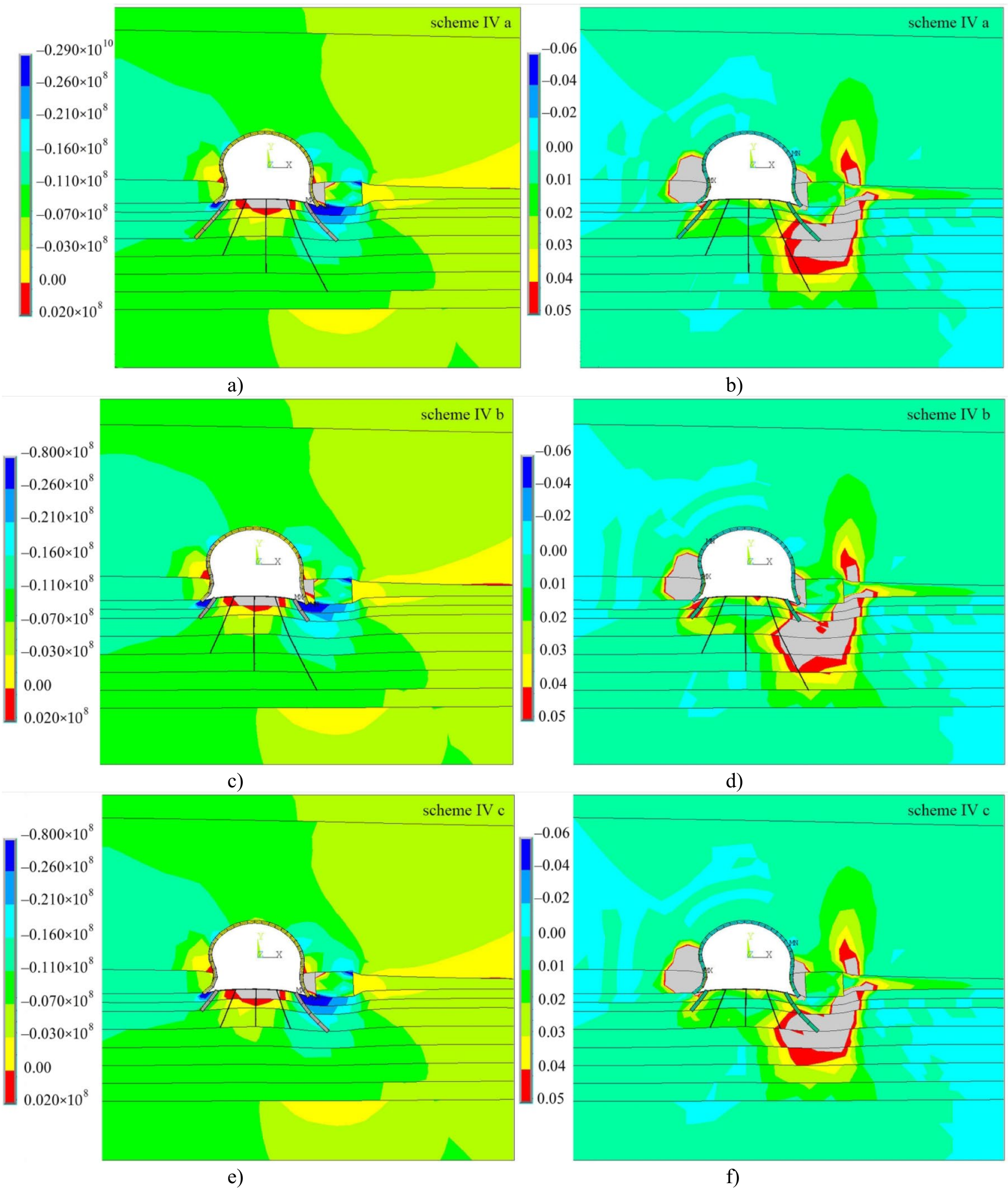

Fig. 19 **a**, **c**, **e** Maximum principle stress and **b**, **d**, **f** Maximum principle strain distributions around the roadway at 6th simulation step after reinforcement with scheme IV

time, extrusion of rocks from under the filling wall body had significant impact;

– vertical delamination of floor strata in the post-peak strains zone under the roadway span and filling wall body.

(2) The floor heave mechanism in gob-side entry retaining is the following one. The concentration of vertical stresses leads to the failure of the coal body on one side of the roadway. On the opposite side of the roadway vertically pressured filling wall body leads to the failure of immediate floor underneath it. As a result, horizontal stress increases in the floor strata that causes the extrusion of rocks from under the filling wall into the entry cavern. In addition, vertical delamination of rocks occurs that provokes a critical floor heave.

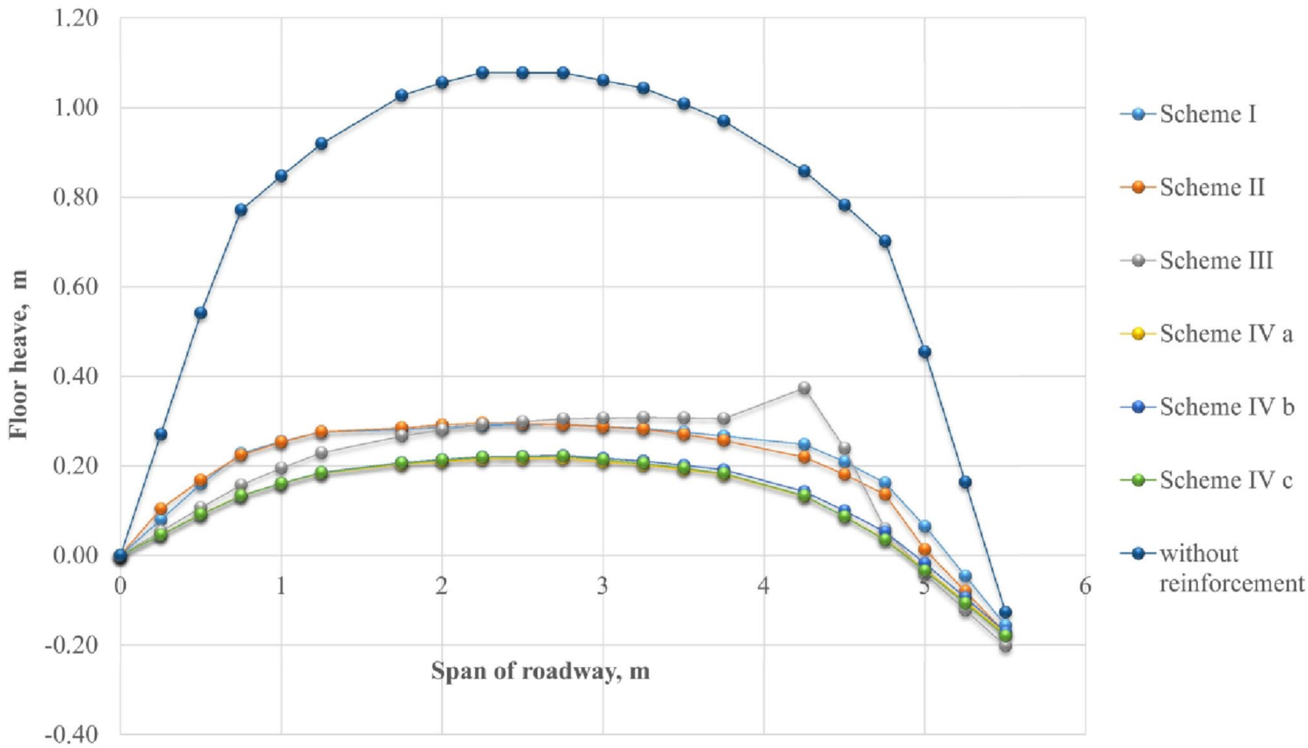

Fig. 20 The roadway floor heave at 6th simulation step after reinforcement with different scheme

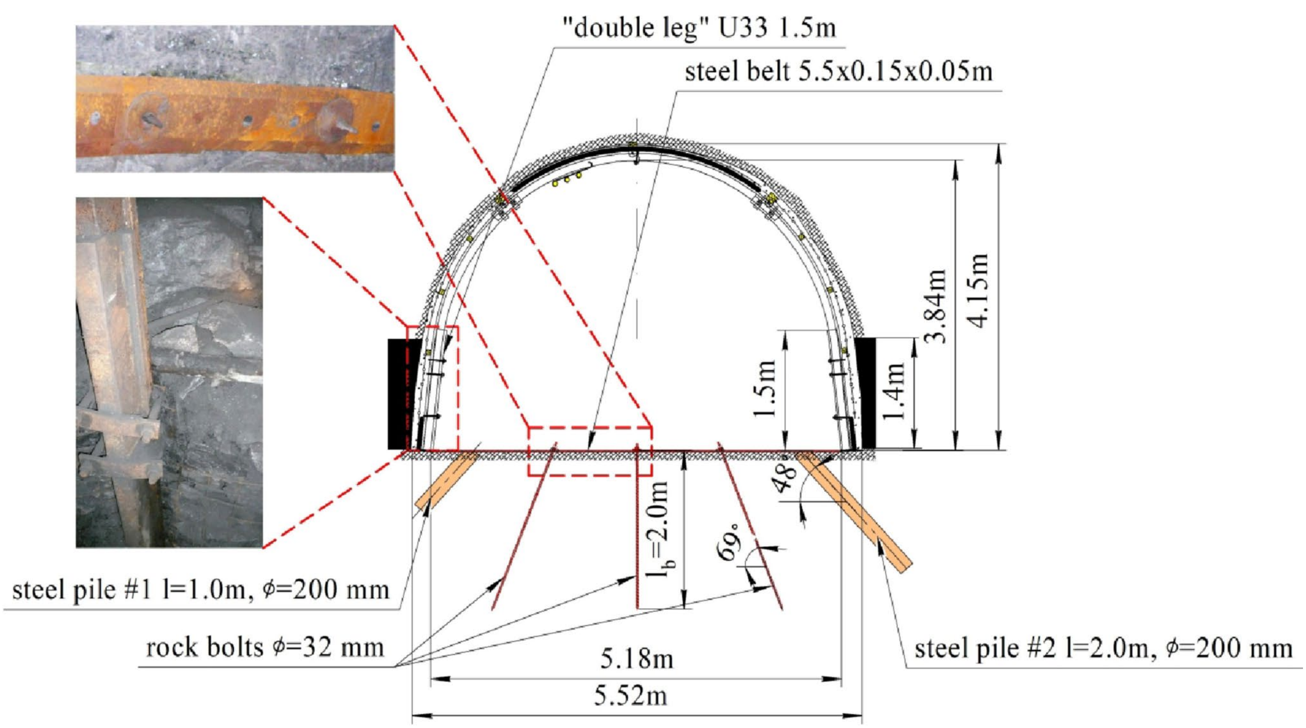

Fig. 21 Design of support scheme

(3) The key to floor heave control in gob-side entry retaining is the resistance to the expansion of rocks in the post-peak strains zone under the roadway span and filling wall, as well as counteraction to horizontal stresses, which were transmitted from the sides of the roadway. Rock bolts-steel piles coupling support technology is the most effective because positive effects of bolts and piles complement each other. As a result, the post-peak strain and stress areas are the smallest, and floor heave reduces by 80%. Among the coupled schemes, the most rational is scheme IVc. In this scheme bolts and one of the steel piles are shorter than in other schemes.
(4) The parameters of the reinforcement scheme must be set in each case separately, depending on the properties of the rocks, parameters of U-shaped steel support, filling wall material and mining depth. For this, it is necessary to analyze the stress and strain distributions around the entry. In this case, the maximum principle strains analysis plays a key role. It can provide guidance for setting optimal parameters for controlling the floor heave.

This research will aid in comprehending the floor heave characteristics in gob-side entry retaining at great depth, paving the way for theoretical groundwork for new bolts-steel piles coupling support methods and their application. The calculation of the parameters of rock bolts-steel piles coupling floor support technology in different geological conditions can be performed by obtaining findings and implementing the proposed suggestions. This will allow to adapt the proposed method to different coal mines.

Funding This research did not receive any specific grant from funding agencies in the public, commercial, or not-for-profit sectors.

Declarations

Conflict of interest The authors declare that they have no known competing financial interests or personal relationships that could have appeared to influence the work reported in this paper.

Contributions Contributions Ivan Sakhno: Investigation, Methodology, Software, Visualization, Writing—Original Draft. Svitlana Sakhno: Investigation, Conceptualization, Writing—Review & Editing.hhhh

References

Abdulla M, Sousa RL, Arzuaga I, Aldajani O, Einstein HH (2021) Fracprop: stochastic fracture propagation model. Rock MechRock Eng 54(5):2513–2531
Almisned OA, Alqahtani N (2021) Rock analysis to characterize Saudi soft sandstone rock. J Petrol Explor Prod Technol 11(6):2381–2387. https://doi.org/10.1007/s13202-021-01160-y
Bieniawski ZT (1989) Engineering rock mass classifications. Wiley, New York, NY, USA
Cao R, Cao P, Lin H (2016) Support technology of deep roadway under high stress and its application. Int J Min Sci Tec 26(5):787–793. https://doi.org/10.1016/j.ijmst.2016.05.046
Chang Q, Zhou H, Xie Z, Shen S (2014) Anchoring mechanism and application of hydraulic expansion bolts used in soft rock roadway floor heave control. Int J Rock Mech Min Sci 23(3):323–328. https://doi.org/10.1016/j.ijmst.2013.05.017
Chen Y, Bai J, Yan S, Xu Y, Wang X, Ma S (2012) Control mechanism and technique of floor heave with reinforcing solid coal side and floor corner in gob-side coal entry retaining. Int J Min Sci Tec 22(6):841–845. https://doi.org/10.1016/j.ijmst.2012.12.002
Deng Z, Zhou L, Zhu Z, Ma L, Chen J, Dai F, Peng T (2024) Study of the fracture properties of twin tunnel surrounds subjected to the coupling of dynamic and static loads. Theor Appl Fract Mech 130:104308. https://doi.org/10.1016/j.tafmec.2024.104308
Deng Z, Zhu Z, Zhou L, Ma L, Huang J, Zhang Y (2024) Effect of dynamic loading orientation on fracture properties of surrounding rocks in twin tunnels. J Rock Mech Geotech Eng 16(2):393–409. https://doi.org/10.1016/j.jrmge.2023.06.017
Faria Santos C, Bieniawski ZT (1989) Floor design in underground coal mines. Rock Mech Rock Eng 22(4):249–271
Gao Y, Wang Y, Yang J, Zhang X, He M (2019) Meso- and macroeffects of roof split blasting on the stability of gateroad surroundings in an innovative nonpillar mining method. Tunn Undergr Space Technol 90:99–118. https://doi.org/10.1016/j.tust.2019.04.025
Gong P, Ma Z, Ni X, Zhang RR (2017) Floor heave mechanism of gob-side entry retaining with fully-mechanized backfilling mining. Energies 10:2085. https://doi.org/10.3390/en10122085.
He MC, Zhang GF, Wang GL, Xu YL, Wu CZ, Tang QD (2009) Research on mechanism and application to floor heave control of deep gateway. Chin J Mech Eng 28:2593–2598
Hoek E, Carranza-Torres C, Corkum B (2002) Hoek-Brown failure criterion—2002 edition. In: Proceedings of the 5th North American Rock Mechanics Symposium and the 17th Tunnelling Association of Canada Conference, NARMS-TAC, Toronto, Canada, ed. Hammah; pp. 267 – 71
Hoek E, Diederichs M (2006) Empirical estimates of rock mass modulus. Int J Rock Mech Min Sci 43:203–215. https://doi.org/10.1016/j.ijrmms.2005.06.005
Josh M, Esteban L, Delle Piane C, Sarout J, Dewhurst DN, Clennell MB (2019) Laboratory characterisation of shale properties. J. Pet. Eng 88:107–24. https://doi.org/10.1016/j.petrol.2012.01.023
Li J, Huang Y, Zhai W, Li Y, Ouyang S, Gao H, Li W, Ma K, Wu L (2020) Experimental study on acoustic emission of confined compression of crushed gangue under different loading rates: disposal of gangue solid waste. Sustainability 12(9):3911. https://doi.org/10.3390/su12093911
Li Z, Zhang Y, Ma Q, Zheng Y, Song G, Yan W, Zhang Y, Hu L (2023) The floor heave mechanism and control technology of gob-side

entry retaining of soft rock floor. Sustainability 15(7):6074. https://doi.org/10.3390/su15076074
Liu Q, Liang B, Sun W, Zhao H (2021) Experimental study on the difference of shale mechanical properties. Adv Civil Eng 2021:6677992. https://doi.org/10.1155/2021/6677992
Liu Q, Fu Q, Yang K, Wei Q, Liu H, Wu H (2022) Geomechanical modeling and inversion analysis of the in-situ stress field in deep marine shale formations: a case study of the Longmaxi Formation, Dingshan Area, China. Front Earth Sci 9:808535
Małkowski P, Ostrowski Ł, Bednarek Ł (2020) The effect of selected factors on floor upheaval in roadways-in situ testing. Energies 13(21):5686. https://doi.org/10.3390/en13215686
Małkowski P, Ostrowski Ł, Stasica J (2022) Modeling of floor heave in underground roadways in dry and waterlogged conditions. Energies 15(12):4340. https://doi.org/10.3390/en15124340
Mo S (2020) A new coal mine floor rating system and itsapplication to assess the potential of floor heave. Int J Rock Mech Min Sci 128:104241. https://doi.org/10.1016/j.ijrmms.2020.104241
Mo S, Ramandi HL, Oh J et al (2018) A Review of Floor Heave Mechanisms in Underground Coal Mine Roadways. The Fourth Australasian Ground Control in Mining Conference. Sydney, New South Wales: The Australasian Institute of Mining and Metallurgy; pp. 196–206
Sakhno I, Sakhno S (2023) Numerical studies of floor heave control in deep mining roadways with soft rocks by the rock bolts reinforcement technology. Adv Civil Eng 2023:2756105. https://doi.org/10.1155/2023/2756105
Sakhno IG, Molodetskyi AV, Sakhno SV (2018) Identification of material parameters for numerical simulation of the behavior of rocks under true triaxial conditions. Naukovyi Visnyk NHU 5:48–53. https://doi.org/10.29202/nvngu/2018-5/4
Shimada H, Hamanaka A, Sasaoka T, Matsui K (2014) Behaviour of grouting material used for floor reinforcement in underground mines. Int J Min Reclam Environ 28(2):133–148. https://doi.org/10.1080/17480930.2013.804257
Tian Z, Zhang Z, Deng M, Yan S, Bai J (2020) Gob-Side entry retained with soft Roof, Floor, and seam in thin coal seams: a casestudy. Sustainability 12:1197. https://doi.org/10.3390/su12031197
Wang C, Chen XY, Zhang JD, Wu YP (2020) Stability mechanism and repair method of U-shaped steel reverse arch support in soft floor roadway. Adv Civil Eng 2020:8814365. https://doi.org/10.1155/2020/8814365
Wang Y, Wang P, Li W, Bai J (2022) Floor heave control technology in deep and soft rock mining roadway: a case study. Arab J Geosci 15:500. https://doi.org/10.1007/s12517-022-09765-1
Xu Y, Chen J, Bai J (2016) Control of floor heaves with steel pile in gob-side entry retaining. Int J Min Sci Technol 26(3):527–534. https://doi.org/10.1016/j.ijmst.2016.02.024
Yang J, Zhou K, Cheng Y, Gao Y, Wei Q, Hu Y (2019) Mechanism and control of roadway floor heave in the paleogene soft rock surroundings. Geotech Geol Eng 37(6):5167–5185. https://doi.org/10.1007/s10706-019-00970-6
Yong C, Bai J, Shuai Y, Ying X, Wang X, Ma S (2012) Control mechanism and technique of floor heave with reinforcing solid coal side and floor corner in gob-side coal entry retaining. Int J Min Sci Technol 22:832–836. https://doi.org/10.1016/j.ijmst.2012.12.002
Yu G, Wang J, Hu J, Zhu D, Sun H, Ma X, Ming W, Li W (2021) Innovative control technique for the floor heave in goaf-side entry retaining based on pressure relief by roof cutting. Math Probl Eng 2021:7163598. https://doi.org/10.1155/2021/7163598
Zhai XX, Qin LT, Chen CY (2017) Combined supporting technology of anchoring and grouting and floor relief in deep chamber of belt conveyor. Chin J Undergr Space Eng 5:1363–1372. https://doi.org/10.3390/en11010067
Zhang X., He M., Yang J., Wang E., Zhang J., Sun Y. Aninnovative non-pillar coal-mining technology with automatically formed entry: a case study. Engineering. 2020; 6(11):1315-1329. https://doi.org/10.1016/j.eng.2020.01.014
Zhang ZY, Shimada H (2018) Numerical study on the effectiveness of grouting reinforcement on the large heaving floor of the deep retained goaf-side gateroad: a case study in China. Energies 11:1001. https://doi.org/10.3390/en11041001
Zheng W, Zhao Y, Bu Q (2018) The coupled control of floor heave based on a composite structure consisting of bolts and concrete antiarches. Math Probl Eng 3545423. https://doi.org/10.1155/2018/3545423
Zhou H, Zhang C, Li Z, Hu D, Hou J (2014) Analysis of mechanical behavior of soft rocks and stability control in deep tunnels. J Rock Mech Geotech Eng 6(3):219–226. https://doi.org/10.1016/j.jrmge.2014.03.003